iScience

CellPress
OPEN ACCESS

Article

CBX7C•PHC2 interaction facilitates PRC1 assembly and modulates its phase separation properties

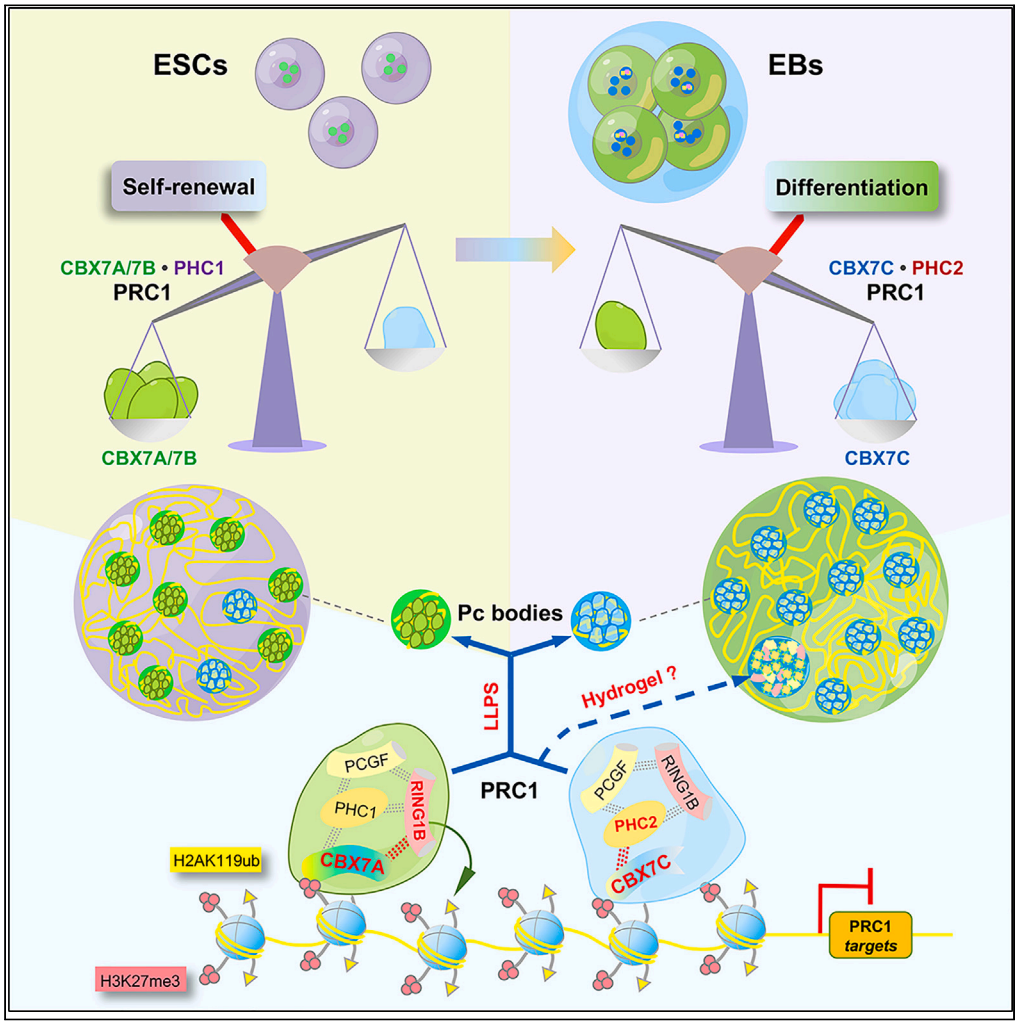

Shanli Guan, Jiajia Tang, Xiaojun Ma, Ruidong Miao, Bo Cheng

bocheng@lzu.edu.cn

Highlights

Cbx7C is a novel *Cbx7* splicing isoform specifically expressed in mouse ESCs

CBX7C recruits RING1B via PHC2 and is able to assemble functional PRC1

The phase separation properties of CBX7C is drastically enhanced by PHC2

CBX7C is upregulated and plays an essential role during mESC differentiation

Guan et al., iScience 27, 109548
April 19, 2024
https://doi.org/10.1016/j.isci.2024.109548

iScience

CellPress
OPEN ACCESS

Article

CBX7C•PHC2 interaction facilitates PRC1 assembly and modulates its phase separation properties

Shanli Guan,[1] Jiajia Tang,[1] Xiaojun Ma,[1] Ruidong Miao,[1] and Bo Cheng[1,2,3,*]

SUMMARY

CBX7 is a key component of PRC1 complex. *Cbx7C* is an uncharacterized *Cbx7* splicing isoform specifically expressed in mouse embryonic stem cells (mESCs). We demonstrate that CBX7C functions as an epigenetic repressor at the classic PRC1 targets in mESCs, and its preferential interaction to PHC2 facilitates PRC1 assembly. Both *Cbx7C* and *Phc2* are significantly upregulated during cell differentiation, and knockdown of *Cbx7C* abolishes the differentiation of mESCs to embryoid bodies. Interestingly, CBX7C·PHC2 interaction at low levels efficiently undergoes the formation of functional Polycomb bodies with high mobility, whereas the coordination of the two factors at high doses results in the formation of large, low-mobility, chromatin-free aggregates. Overall, these findings uncover the unique roles and molecular basis of the CBX7C·PHC2 interaction in PRC1 assembly on chromatin and Pc body formation and open a new avenue of controlling PRC1 activities via modulation of its phase separation properties.

INTRODUCTION

Polycomb group (PcG) proteins are well-known epigenetic repressors essential for the formation and maintenance of "cell memory" in the process of stem cell differentiation. They are often organized into two protein complexes, PRC1 and PRC2, and both complexes function coordinately as histone writers and readers to drive the formation of facultative heterochromatin.[1–5] PRC2 is responsible for catalyzing the trimethylation at H3K27 positions around the targeted chromatic regions.[6–8] All the subtypes of PRC1 (PRC1.1∼PRC1.6) share the catalytic component RING1B (or RING1A) and generate the mono-ubiquitination of H2AK119 on the adjacent nucleosomes.[9,10] The canonical PRC1 (cPRC1) subtypes are specified by the inclusion of one of the five mammalian orthologs for fly Pc protein (CBX2, 4, 6, 7, 8), which recognizes and binds to H3K27me3.[3,11–14]

In the current model, the chromatin-targeting process of cPRC1 mainly depends on the chromodomain-containing CBX family protein to recognize the H3K27me3 marks,[3,11–14] followed by the sequential assembly of the whole complex on the targeted chromatin via the intermolecular interactions among the core components (Figure S1A). The conserved Pc box (PC) at the C-terminus of the CBX protein directly interacts to the RAWUL domain at the C-terminus of RING1B, harboring the E3 ubiquitin ligase activity, serving as a heterodimeric core to drive the complex assembly[15–18] (Figure S1B). However, when the H3K27me3 mark was diminished by knocking out the essential PRC2 component, EED, the chromatin association of CBX7 was largely unaffected,[19] which was consistent with the recent report that JARID2-PRC2.2 subcomplex had a weaker catalytic activity for H3K27me3 and was responsible for the recruitment of CBX7-cPRC1.[20] These findings emphasize that the delicate targeting and assembly mechanisms of cPRC1 remain to be further explored.

Another layer of complexity comes from the alternative splicing-associated protein isoforms of the PRC1 components. For example, human *CBX2* was reported to produce an alternative splicing isoform due to the change of an intron/exon boundary, and the resultant PC-less CBX2 isoform remained functioning as an epigenetic repressor via unknown working mechanisms.[21] The *Cbx4* and *Cbx6* of zebrafish also encode PC-less isoforms.[22] In addition, there are three annotated splicing isoforms for the mouse *Cbx7* locus (http://genome.ucsc.edu, mouse genome NCBI37/mm9 version), namely *Cbx7A*, *Cbx7B*, and *Cbx7C* for easy distinguish, and among them *Cbx7C* produces an uncharacterized PC-less CBX7C protein. The prevalent existence of the PC-less CBX isoforms in metazoans suggests that these CBX variants may assemble specialized PRC1 subtypes or play important regulatory roles for their full-length counterparts. The conserved PC domain is responsible for mediating RING1B binding and therefore important for PRC1 assembly.[18,23] Theoretically, the PC-less CBX proteins may fail to assemble into functional PRC1, meanwhile competing with its functionally competent counterparts for binding to the target genes. The molecular properties and functions of the PC-less mouse CBX7C isoform have not been explored, presumably due to its low expression. Thus, in this study, we mainly explored the molecular properties and functions of CBX7C, focusing on its unique working mechanisms in cPRC1 assembly and the subsequent phase separation.

[1]School of Life Sciences, Lanzhou University, Lanzhou 730000, Gansu, P.R. China
[2]Key Laboratory of Cell Activities and Stress Adaptations, Ministry of Education, Lanzhou University, Lanzhou 730000, Gansu, P.R. China
[3]Lead contact
*Correspondence: bocheng@lzu.edu.cn
https://doi.org/10.1016/j.isci.2024.109548

It has been well known that polycomb proteins tend to form membrane-less nuclear condensates, namely Polycomb bodies (Pc bodies), which dynamically regulate the three-dimensional genomic structures and facilitate the co-repression of multi-targets via mediating the long-distance chromatin interactions and compaction.[15,16,24,25] The intrinsically disordered regions (IDRs) of CBX2 play an important role to trigger liquid-liquid phase separation (LLPS) of the Pc bodies.[26,27] In addition, the PHC2 protein in cPRC1 is also associated with phase separation, which is contributed by both its C-terminal SAM domain and the N-terminal IDRs.[28–33] Although CBX7 is the dominant CBX protein in mESCs, its intrinsic phase separation capability seemed to be relatively weak compared with CBX2, suggesting that CBX2 plays a key role in the initial formation of Pc bodies during early embryogenesis.[15,34,35] In the process of cell fate transition, the dynamic changes of chromatin structures are closely related to the changes of gene expression and are tightly associated with diseases when misregulated.[36,37] However, so far it remains unclear whether and how the phase separation properties of PRC1 can be precisely controlled by the developmental program.

In this study, we confirmed the expression of CBX7C in mESCs and dissected its molecular properties in PRC1 assembly and Pc body formation. Our data indicated that CBX7C indeed lost its direct interaction to RING1B, whereas it remained capable of PRC1 assembly at the known PRC1 targets via an alternative PHC2-dependent strategy. Strikingly, the intrinsic phase separation capabilities of CBX7C were dramatically enhanced in the presence of PHC2, and with the increase of the CBX7C•PHC2 interaction, they tended to generate large, chromatin-free aggregates containing all the cPRC1 components. In addition, we identified the regions CBX7 or PHC2 via mutant analyses that were responsible for their direct interaction, Pc body formation, and abnormal condensation. The expression of *Cbx7C* in mESCs was particularly interesting because CBX7 was found as the dominant member among the CBX family members for cPRC1 assembly in mESCs and later replaced by the other CBX proteins upon differentiation.[38] Our data indicated that CBX7C and PHC2 were expressed in mESCs at low levels, whereas they were both upregulated significantly upon differentiation, which was consistent to the downregulation of PRC1 activities during this cell fate transition. RNAi data further revealed that CBX7C played an essential role for the differentiation process from mESCs to embryoid bodies. Overall, this study identified a specialized CBX7C-containing cPRC1 subtype in mESCs and proposed a detailed working model that relied on the CBX7C•PHC2 interaction to drive cPRC1 assembly and to modulate the phase separation status of the cPRC1-containing polycomb proteins in a dose-dependent manner.

RESULTS

Cbx7C is a *Cbx7* isoform specifically expressed in mESCs and in certain mouse tissues

The splicing patterns of all three *Cbx7* isoforms are shown in Figure 1A. We set out to examine their expression profiles in mESCs and various mouse tissues. The RT-qPCR results indicated that all three isoforms were expressed in mESCs (Figures 1B and 1C). Although the expression level of *Cbx7C* was much lower than *Cbx7A* or *Cbx7B*, it was clearly detectable in mESCs and in specific mouse tissues, such as spleen and testis. Meanwhile, *Cbx7C* was also expressed in the mouse teratocarcinoma F9 cells (Figure S2A). A rabbit polyclonal antibody against the unique region of CBX7C (amino acids 83–166) was generated and verified (Figure S2B). Western blotting analyses showed that *Cbx7C* produced a protein with an expected size around 20 kDa (Figure 1D), and the identity of this protein was also verified via RNAi assays (Figure S2C). The abovementioned data confirm that *Cbx7C* is a protein coding *Cbx7* isoform specifically expressed in mESCs, F9 cells, and certain tissues.

CBX7C loses RING1B-binding activity yet remains present in enzymatically active cPRC1 in mESCs

Based on the known information about domain interaction, missing the PC domain in CBX7C will cause a loss of the direct interaction to RING1B and may change its interaction pattern to the other cPRC1 components. We next carried out BiFC experiments to examine the interactions between CBX7 isoforms and the cPRC1 components highly expressed in mESCs, including RING1B, PHC1, and PCGF2 (Figures 1E and S2D). The results confirmed that CBX7C lost the interaction to RING1B. None of the three CBX7 proteins generated positive BiFC signals with PCGF2, consisting to the reported PRC1 assembly model where CBX proteins did not directly interact to PCGF proteins.[39] Although PHC1 was expressed at a much higher level than PHC2 in mESCs (Figure S2E), interestingly, we found that all three CBX7 isoforms interacted to PHC2 but not PHC1, suggesting that the conformation of PHC2 in PRC1 complex might be more beneficial for setting up the interaction to CBX7. It was reported that the small amount of PHC2 expressed in mESCs worked synergistically with PHC1 in transcriptional repression.[40,41] Therefore, in this study we focused more on PHC2 than PHC1.

The abovementioned BiFC interactions were further verified via GST-pull down assays. Here, we chose CBX7A as a full-length counterpart for parallel comparisons with CBX7C, because it covered the entire sequences and shared very similar epigenetic regulatory properties with CBX7B (Figures S2F and S2G). The data further prove that CBX7C indeed loses the direct interaction to RING1B and meanwhile both CBX7A and CBX7C interact directly to PHC2 *in vitro* (Figure 1F).

Next, we tested the capabilities of CBX7C in cPRC1 assembly at target genes and transcriptional repression in mESCs. The physiological interactions of CBX7C to the core cPRC1 components were detected via co-immunoprecipitation (co-IP) assays in an mESC line inducibly expressing CBX7C. Different from the data of BiFC and GST pull-down assays shown earlier, the co-IP results indicated that CBX7C was able to precipitate both RING1B and PCGF2 (Figure 2A). In addition, ChIP-qPCR analyses indicated that the ectopically expressed CBX7C, induced by doxycycline (Dox) in mESCs, was enriched at those classical cPRC1 target genes, and the binding of CBX7C on those loci often reduced the association of CBX7A or 7B, suggesting that CBX7C competed binding with the other isoforms at the target genes (Figure 2B). On the contrary, there was a general upward trend for the enrichment signals of PCGF2 and RING1B at the majority of genes tested, and consistently, the resultant H2AK119ub modification was also increased (Figure 2B). Overall, these data suggest that CBX7C competes with CBX7A and 7B for binding on their target genes, whereas the integrity and the enzymatic activities of the cPRC1 complexes are well sustained. Furthermore, the transcription levels of the CBX7C-containing cPRC1 bound genes were frequently downregulated (Figure 2C),

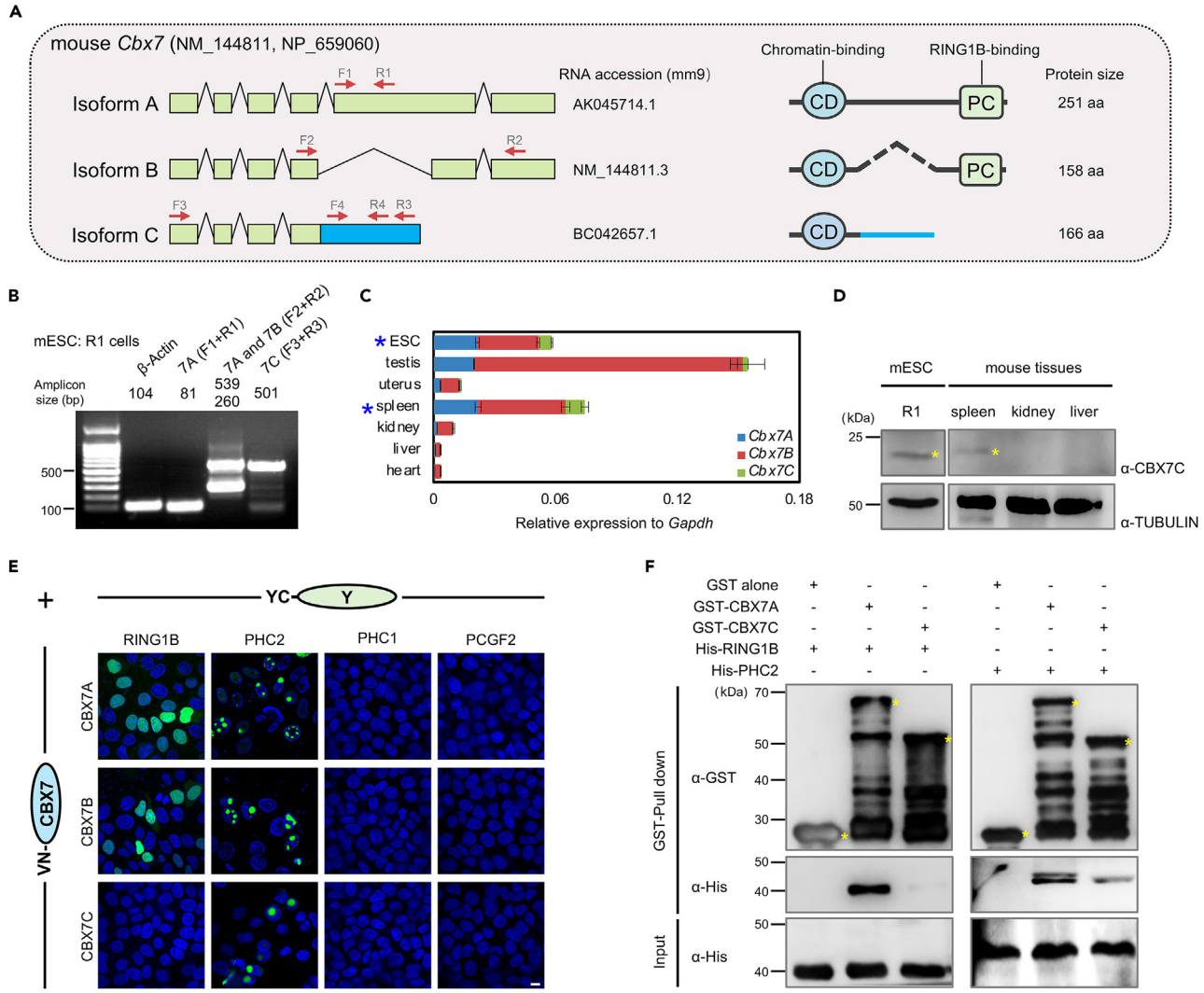

Figure 1. Mouse *Cbx7C* is a *Cbx7* splicing isoform that specifically expressed in mESC and certain tissues

(A) The basic information of the three mouse *Cbx7* isoforms and the protein products.

(B) The RT-qPCR analyses of the expression of *Cbx7* isoforms in mESCs. The primer pairs used in each PCR reaction were indicated on the top of the gel and labeled in (A).

(C) RT-qPCR analyses of the expression of the three *Cbx7* isoforms in the indicated mouse tissues. Data are represented as mean ± SD.

(D) Western blotting analyses of the expression levels of CBX7C in mESCs and in the indicated mouse tissues. The asterisk indicated the position of the CBX7C bands.

(E) BiFC analyses and the confocal images of the interaction between each CBX7 isoform and the indicated PRC1 components in HeLa cells. Scale bar, 10 μm.

(F) GST-pull-down analyses between CBX7A or CBX7C and RING1B or PHC2. The asterisks point out the intact band of the indicated protein.

and the transcriptional repression capabilities of CBX7C, CBX7A, and PHC2 were assessed and proved in the reporter assays (Figure 2D). These results reveal that CBX7C is capable of competing with CBX7A or CBX7B in assembling cPRC1 with the transcriptionally repressive activity at their common targets in mESCs.

CBX7C is capable of driving the *de novo* assembly of functional cPRC1 on chromatin

Although CBX7C was found to be enriched at cPRC1 target genes, it remained unclear whether it acted as a "driver" or it was passively recruited as a "passenger" during the assembly process of cPRC1. Usually, PRC1 and PRC2 complexes and their corresponding modifications of H2AK119ub and H3K27me3 are enriched at the facultative heterochromatin regions.[4,5] Hereby, we employed a heterochromatin targeting module (HTM)-mediated artificial tethering system to identify the potential driver(s) in the assembly of cPRC1. Each candidate was fused with an mCherry tag and an 88 aa, HTM motif cloned from the H4K20 methyltransferase, SUV420H2. The resultant fusion protein would

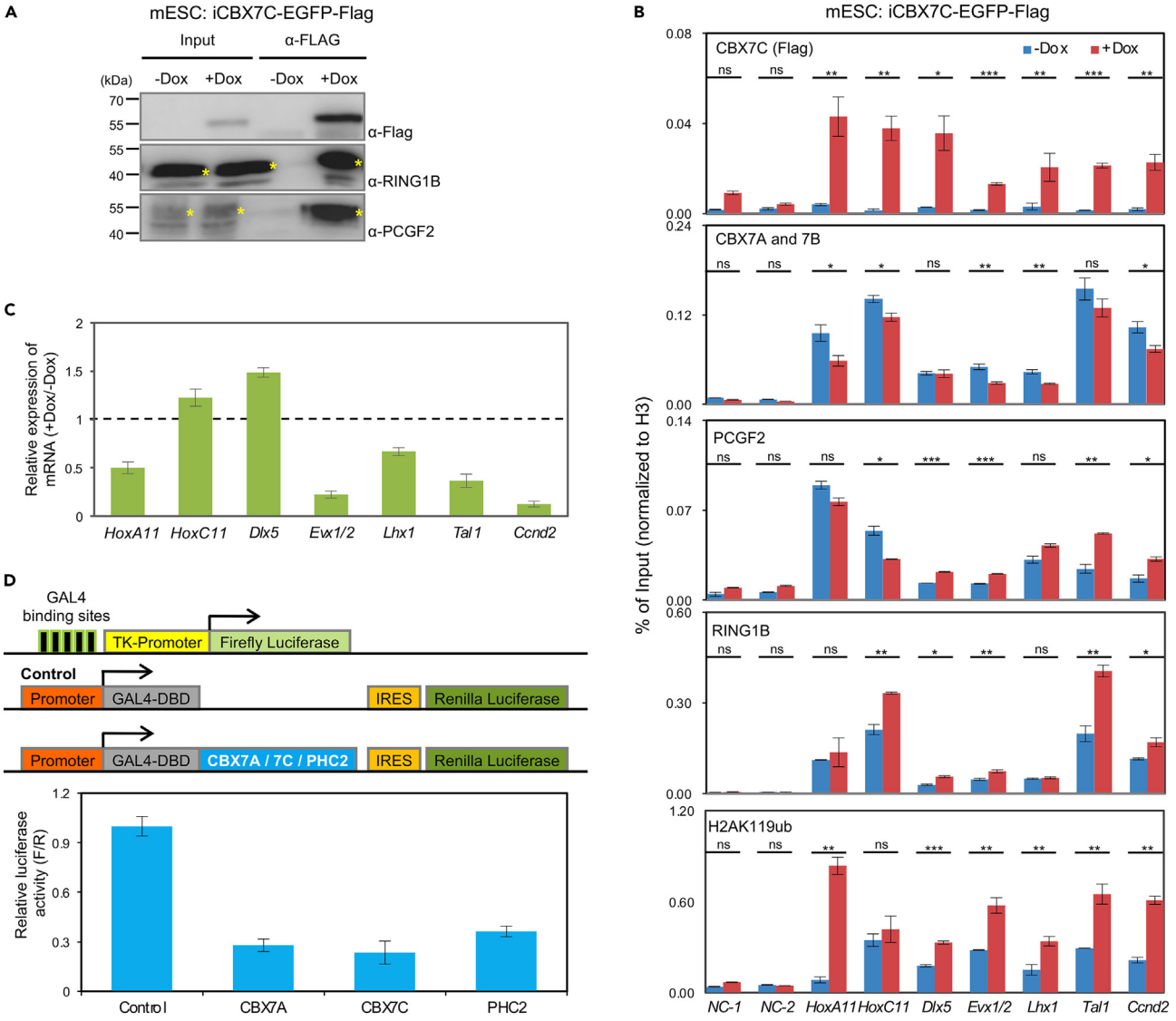

Figure 2. The molecular interactions and functions of CBX7C in mESCs

(A) The co-IP analyses of the interactions between CBX7C and the indicated PRC1 components in the mESCs cell line inducibly expressing CBX7C (mESC: iCBX7C-EGFP-Flag). The asterisks indicate the bands of RING1B and PCGF2.

(B) Examination of the enrichment of the indicated proteins or histone modifications at the classical PRC1 target genes. ChIP-qPCR analyses of the enrichment of CBX7C-EGFP-Flag at the indicated known cPRC1 target genes and the effects on the enrichment of other PRC1 components or H2AK119ub at these loci in the stable mESC line. NC-1 (*Myc*) and NC-2 (*Klf4*) were the confirmed negative controls in mESCs. The statistical graph represents the ChIP-qPCR results (significant differences between means were determined using Student's t test: ns, not significant, $p > 0.05$; *$p < 0.05$; **$p < 0.01$; ***$p < 0.001$).

(C) RT-qPCR analyses of the expression of the selected PRC1 target genes are shown in (B).

(D) Dual luciferase assays testing the effects of CBX7A, CBX7C, or PHC2 on the reporter expression. HEK293T cells stably expressing the Firefly luciferase were transfected with a plasmid expressing GAL4-DBD alone or fused with the indicated PRC1 component. The levels of the Renilla luciferase were used for data normalization. Data in (B–D) are represented as mean ± SD.

be tethered at the constitutive heterochromatin regions featured with H3K9me3 and H4K20me3.[5,21,42] Compared with the published TetR-tetO targeting system,[43] which detected the assembly of PRC1 and its regulatory effects on a reporter gene, the tethering system used here focused more on the driver-passenger relationship during the *de novo* assembly process of cPRC1 at chromatin sites outside of its regular territory, detected via fluorescent protein tagging or combining with IF analyses (Figure 3A). The efficiency and specificity of this tethering system were verified upon the expression of mCherry-HTM alone in mESCs, where the mCherry$^+$ condensates were found perfectly overlapped with the H3K9me3-marked constitutive heterochromatin but distinct from the nuclear distribution of the endogenous RING1B or H2AK119ub (Figure S3A).

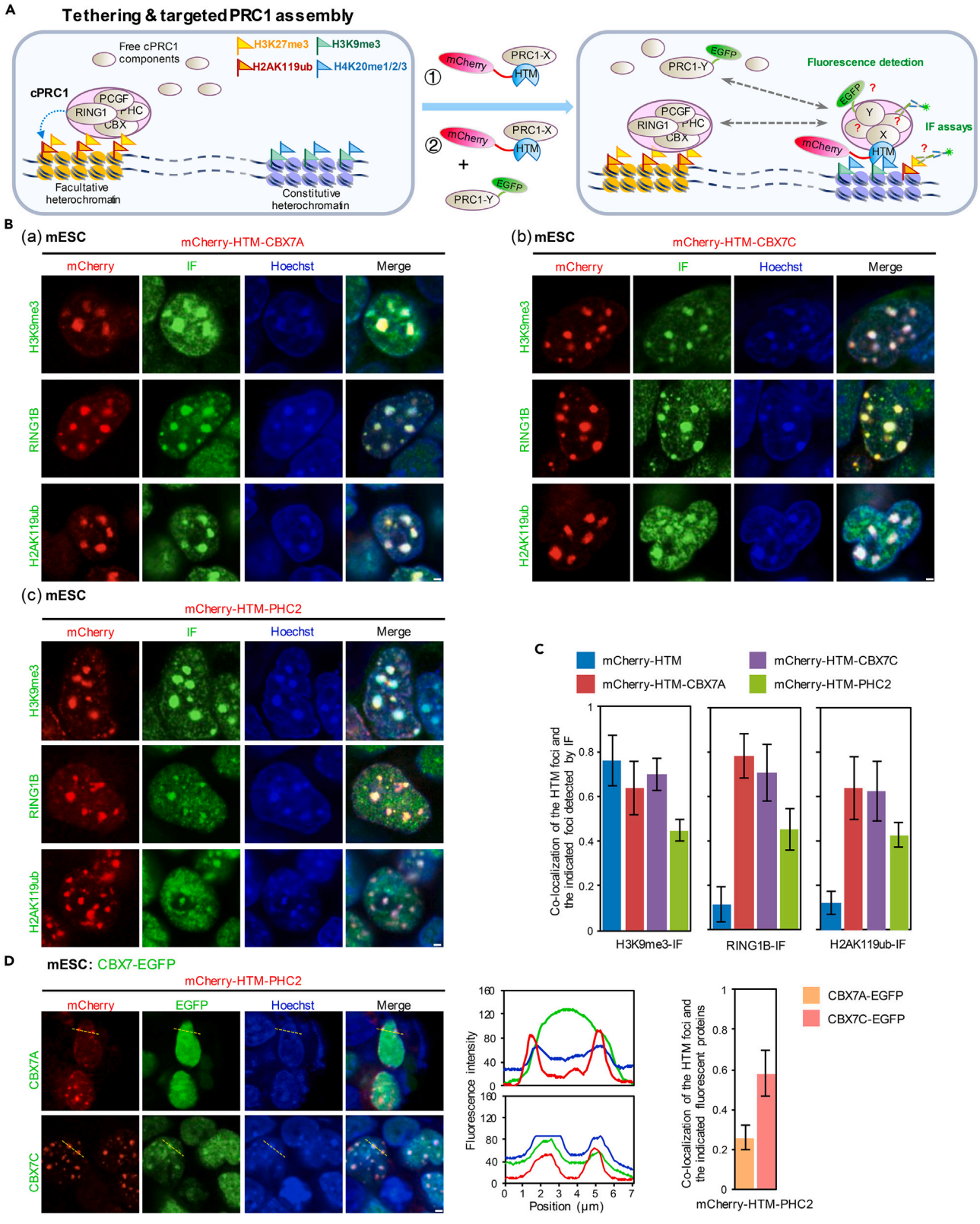
A
Tethering & targeted PRC1 assembly
Free cPRC1 components
H3K27me3
H3K9me3
H2AK119ub
H4K20me1/2/3
cPRC1
PCGF
RING1
PHC
CBX
Facultative heterochromatin
Constitutive heterochromatin
mCherry
PRC1-X
HTM
EGFP
PRC1-Y
Fluorescence detection
IF assays
B
(a) mESC
mCherry-HTM-CBX7A
(b) mESC
mCherry-HTM-CBX7C
mCherry
IF
Hoechst
Merge
H3K9me3
RING1B
H2AK119ub
(c) mESC
mCherry-HTM-PHC2
C
mCherry-HTM
mCherry-HTM-CBX7A
mCherry-HTM-CBX7C
mCherry-HTM-PHC2
Co-localization of the HTM foci and the indicated foci detected by IF
H3K9me3-IF
RING1B-IF
H2AK119ub-IF
D
mESC: CBX7-EGFP
mCherry-HTM-PHC2
EGFP
CBX7A
CBX7C
Fluorescence intensity
Position (μm)
CBX7A-EGFP
CBX7C-EGFP
Co-localization of the HTM foci and the indicated fluorescent proteins
mCherry-HTM-PHC2

Figure 3. Identification of the driver component(s) for PRC1 assembly via the HTM-mediated tethering system

(A) A diagram of the principle of the HTM-based artificial tethering and PRC1 complex assembly assay.

(B) The confocal images detecting the distribution of the foci composed of the mCherry-HTM-CBX7A (a) or CBX7C (b) or PHC2 (c) and their associated histone modifications or the recruited PRC1 components in mESCs.

(C) A bar graph indicates the proportions of the colocalized foci to all the mCherry-HTM-labeled foci shown in (B), quantified by ImageJ (n = 5).

(D) The confocal images detecting the recruitment of CBX7 isoforms by mCherry-HTM-PHC2 in mESCs stably expressing CBX7A-EGFP or CBX7C-EGFP (left). Chromatin was labeled via Hoechst staining. The intensity of various fluorescence across the randomly selected regions (shown as the dashed lines) was scanned and plotted on the right of each image to demonstrate the colocalization status of the indicated factors or modifications (middle). The proportion of colocalized foci to the HTM-tethered foci was quantified by ImageJ (n = 5) and shown in the bar graph on the right. Scale bar, 2 μm in (B and C) and 4 μm in (D). Data in (C–D) are represented as mean ± SD.

Next, we tethered the PRC1 components and monitored the cPRC1 assembly at constitutive heterochromatin. When mCherry-HTM-CBX7A was tested, we observed the colocalization of the endogenous RING1B and the resultant H2AK119ub signals with the mCherry-marked condensates, supporting that CBX7A may act as a "driver" for the recruitment of other components to assemble catalytically active cPRC1 (Figures 3B(a) and 3C). Surprisingly, the mCherry-HTM-CBX7C condensates were also capable of recruiting the endogenous RING1B and generating H2AK119ub (Figures 3B(b) and 3C), even though it lost the RING1B-binding activity. These data prove that similar to CBX7A, CBX7C is also capable of driving the formation of cPRC1 complexes with a competent enzymatic activity.

Considering that PHC2 is capable of binding to both RING1A/1B and CBX7 proteins directly (Figures 1F and S1A), the PC-less CBX7C may indirectly set up contacts with the rest of the core components of cPRC1 through PHC2. Next, we analyzed the potential role of PHC2 in organizing cPRC1 assembly. The result indicated that at least under the tethering conditions, PHC2 could also act as a "driver" to trigger the cPRC1 assembly, although less efficiently than the CBX7 proteins (Figures 3B(c) and 3C). Strikingly, compared with CBX7A, HTM-PHC2 preferentially recruited CBX7C in mESCs (Figure 3D). Because PHC2 has not been found to act as a direct DNA-binding factor or a histone "reader," our data suggest that the PHC2-driven cPRC1 assembly may occur once being recruited to target genes by certain sequence specific transcription factors. The combination of the abovementioned results reveals a mutual recruitment model between CBX7C and PHC2, and this coordinated interaction promotes the further assembly of the intact cPRC1 at target sites.

CBX7C and PHC2 are both upregulated during mESC differentiation, and knockdown of *Cbx7C* abolishes the formation of embryoid bodies

Because *Cbx7C* was expressed at a low level in mESCs, we wondered whether it may play any role during mESC differentiation. The protein levels of CBX7C were detected upon the induction of mESC differentiation and EB formation upon LIF withdrawal. Consistent to the previous report,[44] CBX7A was downregulated upon cell differentiation (Figure 4A). In contrast, our WB results clearly indicated that CBX7C was significantly increased at the same time. For example, on day 6 of EB formation, CBX7C was greatly increased while simultaneously CBX7A was almost disappeared (Figure 4A). Notably, PHC2 was also found increased at early stage (before day 6) although it decreased at later stages (Figure 4A). The fact of the coinduction of CBX7C and PHC2 suggests that they may work together during the early stage of ESC differentiation.

Next, we modulated the expression levels of *Cbx7C* via overexpression or RNAi and examined the corresponding effects on EB formation. The results indicated that the mESCs stably expressing ectopic *Cbx7C* were able to generate embryoid bodies (EBs), and compared with the wild-type mESCs, the CBX7C-EBs generally grew faster and looked more rounded and smoother in shape (Figure 4B). In contrast, upon LIF withdrawal, instead of growing in suspension to form EBs, the mESCs with *Cbx7C* were being knocked down directly attached to the bottom of the dish and underwent abnormal differentiation (Figure 4C). These data indicate that CBX7C serves as a promoting factor required for EB formation during mESC differentiation.

The abovementioned data suggest that CBX7C may compete with CBX7A for PHC2 binding and cPRC1 formation (Figures 3D and 2B). To obtain direct evidence, a set of BiFC competition assays was carried out as follows. Because the transfection efficiency in mESCs was extremely low, the experiments associated with cotransfection of multiple plasmids were carried out in HeLa cells. The two binding partners, CBX7A and PHC2, were constructed in a pair of BiFC plasmids respectively and expressed in cells to generate BiFC signals (green color). The third plasmid expressing the competitor, mCherry-CBX7C, was simultaneously transfected into cells with variable amounts (from 0.2 to 1.6 times of the amounts of the CBX7A plasmid). The competition between CBX7A and CBX7C for PHC2 binding was examined by monitoring the changes of the BiFC and the mCherry signals. As shown in Figures 4D and S3C, with the increased expression of mCherry-CBX7C, the CBX7A•PHC2 BiFC signals were gradually deceased while this phenomenon was not seen when expressing mCherry alone, indicating that CBX7C was efficient in competing with CBX7A for PHC2 binding.

PHC2 and CBX7C coordinately modulate the physical and functional properties of the Pc condensates

PRC1 complexes are known to form Pc bodies in live cells,[45–48] which are membrane-less nuclear condensates generated via phase separation.[49] Both CBX7A or CBX7C generally formed nuclear condensates in stably expressed mESCs (Figure 5A). Accumulating studies have uncovered that the proteins harboring the significant IDRs were prone to form liquid-liquid phase-separated condensates under appropriate cellular conditions, which has been considered as necessary characteristics for the occurrence of phase transition.[50–52] IDR prediction revealed that CBX7A contained six discontinuous IDRs (~70.92% of the entire protein), and similarly, CBX7C

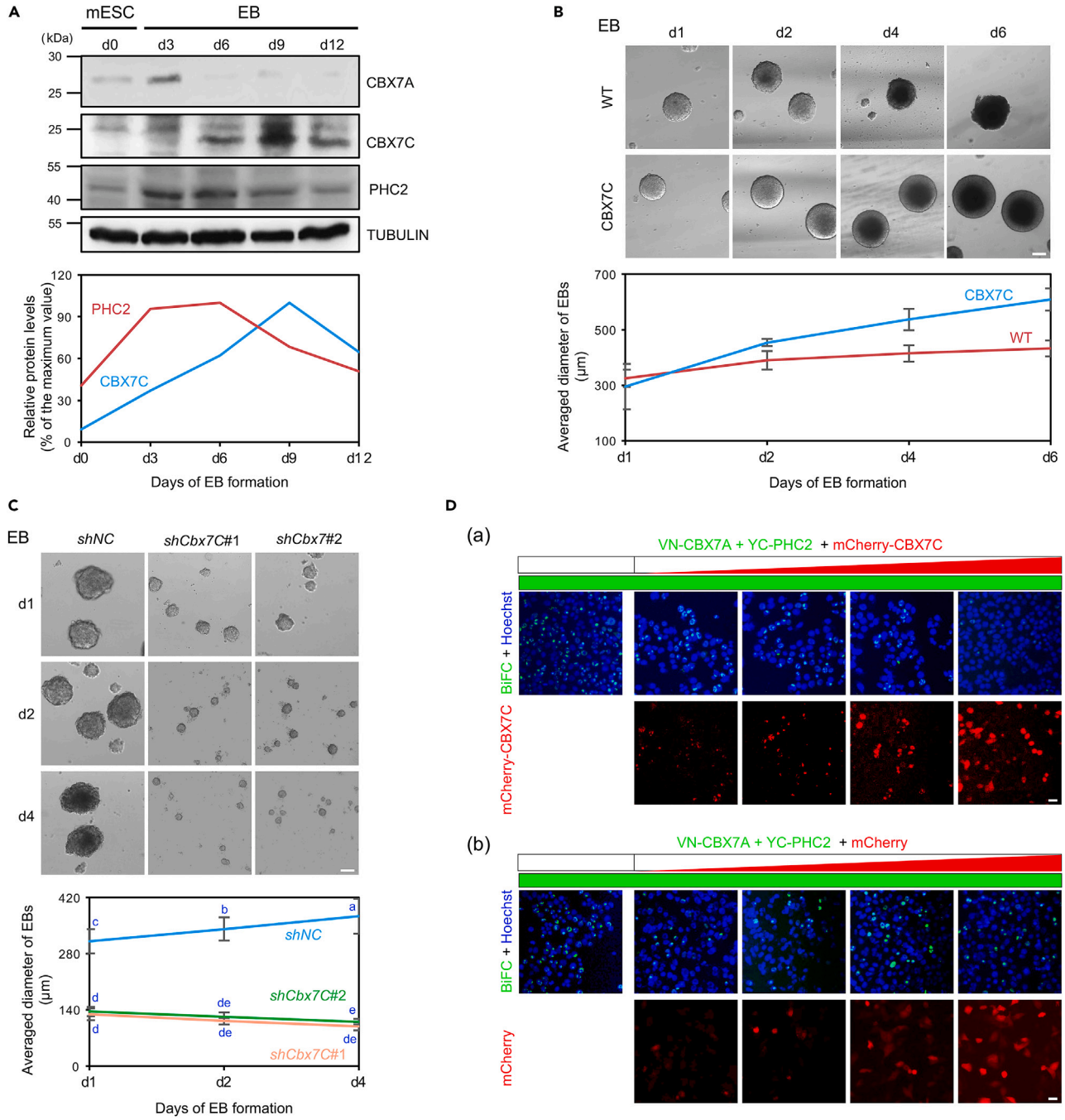

Figure 4. Induced expression of CBX7 and PHC2 during mESC differentiation and the effects of modulating *Cbx7C* expression on EB formation

(A) WB detection of the expression levels of the indicated proteins during EB formation on 0, 3, 6, 9, and 12 days post LIF withdrawal. The data quantification was carried out via gray value analyses, and the relative expression value was shown at the bottom.

(B) Images of EBs (10× magnification) formed by the wild type or mESCs stably expressing CBX7C at the indicated time post LIF withdrawal. Scale bar, 200 μm. The average diameters of the EBs were measured using ImageJ software. All error bars represent the standard error of the mean diameter from at least 12 EBs for each condition.

(C) Images of EBs (10× magnification) formed by mESCs with either the control knockdown (*shNC*) or the *Cbx7C* knockdown (*shCbx7C*#1 or #2) at the indicated time post LIF withdrawal. Scale bar, 200 μm. The average diameters of the EBs were calculated using ImageJ software. All error bars represent the standard error of the mean diameter of EBs for each condition. Different letters indicate significant differences as determined using ANOVA followed by Duncan's multiple range test ($p < 0.05$). Data in (B–C) are represented as mean ± SD.

Figure 4. *Continued*

(D) The competitive interaction between CBX7C and CBX7A for binding to PHC2 detected via BiFC competition experiment. HeLa cells were transiently transfected with the combination of plasmids expressing the indicated proteins. The amounts of the "competitor" plasmid were ranged from 0.2, 0.4, 0.8, and 1.6 times of each one of the BiFC plasmid (400 ng of the indicated plasmid to each well of a 12-well plate). Images at a 10× magnification are shown. Scale bar, 20 μm.

contained four (~69.88% of the total sequence) (Figure S4A), suggesting that both of the CBX7 proteins have the potential to drive phase separation.

To compare the phase separation capabilities of CBX7 isoforms in cells, we adopted an optogenetics-based system, in which the fusion of Cry2 with a typical IDR from a phase separation driver would undergo a rapid blue-light-induced cluster assembly (Figure 5B(a)).[53] mCherry-labeled Cry2 was expressed alone (as a negative control) or further fused with one of the three CBX7 isoforms in HeLa cells, and the occurrence of the blue-light-induced phase separation events was monitored. Without induction, the basal levels of condensates were formed, among which CBX7C generated the highest amount of the condensates (Figure 5B(b and c)). Unlike CBX7A and CBX7C, CBX7B was also expressed partially in the cytoplasm, which was consistent with its subcellular localization in mouse MEF cells shown in previously published article.[54] Upon blue light activation, the quantities of the condensates formed by all the CBX7 isoforms were further increased. Overall, this result indicates that all three CBX7 isoforms have the capability of phase separation to some extent, and the intrinsic phase separation capability of CBX7C seems to be the strongest.

Next, we examined the effects of PHC2 on the phase transition capabilities of CBX7A or CBX7C in HeLa cells. Consistent to the results obtained in mESCs (Figure 3B), tethering CBX7A, CBX7C, or PHC2 alone to the constitutive heterochromatin via an HTM fusion resulted in the formation of the catalytically active Pc condensates (Figures 5C(a) and S4B). The coexpression of CBX7C (or CBX7A) and PHC2 formed much larger condensates with the two proteins perfectly colocalized (Figure 5C(b)). Notably, these huge condensates looked quite different from those catalytically active Pc bodies because they were excluded from the chromatin (Hoechst negative). Similar observation was obtained when HTM-fused PHC2 was coexpressed with "free" CBX7C or CBX7A (Figure S4C). These results indicate that the phase separation capabilities of CBX7C and PHC2 are mutually coordinated. When massive amounts of both factors were present, the HTM-mediated tethering force was completely overcome. In addition, the average sizes of the large condensates formed by CBX7C were much bigger than those made by CBX7A (Figure 5C(c)), which further proved the discovery that the phase separation capability of CBX7C is much potent than CBX7A. Furthermore, we found that PHC2 not only coordinated with CBX7 in promoting the phase transition of Pc condensates but also worked together with other cPRC1 components to achieve similar effects, such as RING1B (Figure S4D). Overall, PHC2 works as a general phase transition enhancer for CBX proteins and potentially other cPRC1 components, and the concentration or strength of their coordinated interaction may determine the status of their phase separation.

Next, we performed the Fluorescence Recovery After Photobleaching (FRAP) assays to compare the intrinsic dynamics of the functional Pc bodies with the large condensates formed by CBX7A/C•PHC2 interaction seen in Figure 5C. It turned out that the fluorescent signals of the chromatin-bound Pc bodies (generated upon the single transfection of mCherry-HTM-CBX7A or CBX7C) were rapidly recovered within a couple of minutes after photobleaching (Figure 5D). This phenomenon of rapid diffusion of these CBX7-containing condensates fit the golden criterion for LLPS condensates.[55,56] In contrast, it took much longer time (>15 min) for the signals within the large condensates to be recovered, and the recovery rates of the CBX7A•PHC2 and CBX7C•PHC2 condensates were about the same (Figures 5D and S4E). These results suggest that the presence of the potent CBX7C/CBX7A•PHC2 interaction will dramatically change the characteristics of the resultant condensates, promoting their agglutination and eventually switching them into a hydrogel state.

Next, we used a live cell imaging system to capture the dynamic formation process of the CBX7C•PHC2 condensates. Figure 5E(a) presented a series of confocal images taken every 3 h from 18 to 27 h post a transient transfection. During this process, the condensates started forming, and their volumes and the fluorescent intensity were gradually increased. Consistent to the phenomenon shown in Figure 5C, the Hoechst signals within the same nuclear regions were simultaneously decreased. Thus, the formation of the large CBX7•PHC2 condensates occurred along with the reorganization of chromatin, and the condensates continuously grew to generate huge chromatin-free areas. Our data from immunofluorescence assays further confirmed the accumulation of all the endogenous cPRC1 core subunits and exclusion of all the histone modifications within these huge condensates (Figures 5E(b and c) and S4F). Interestingly, the immunofluorescence signal of the endogenous CBX7A was excluded and distributed around those CBX7C-containing condensates, further supporting that CBX7C and CBX7A were mutually exclusive in a given cPRC1 complex (Figures 5E(b and c) and S4G). Taken together, these results demonstrate that CBX7C has a potent capability to undergo phase separation, and PHC2 dramatically enhances this property, and the coordinated action of CBX7C and PHC2 strongly controls the phase transition and the functionality of the resultant Pc condensates.

Identification of the regions responsible for the CBX7·PHC2 interaction and their coordinated phase separation

Next, we dissected the key region(s) that mediated the formation of the CBX7•PHC2 dimer in His-pull down assays and compared the differences between CBX7A and CBX7C. Because their interaction properties may be tightly correlated to their phase separation activities, we expressed the N- or C-terminal region of CBX7A or CBX7C, namely $CBX7A_N$ or $CBX7C_N$ or $CBX7A_C$ or $CBX7C_C$, respectively, based on their natural distribution of the IDRs (see details in Figure S4A and the top panel of Figure 6A). The results showed that the N-termini of both CBX7A and CBX7C played a major role in mediating their direct interactions to PHC2, although the C-termini might be involved as well (Figure 6A). In addition, it was reported that the C-terminal SAM domain of PHC2 played an important role in complex polymerization and the LLPS process.[29,32] Thus, we also compared the SAM-deleted PHC2 mutant ($PHC2_{\Delta SAM}$) with the full length ($PHC2_{FL}$) in the CBX7•PHC2 interaction.

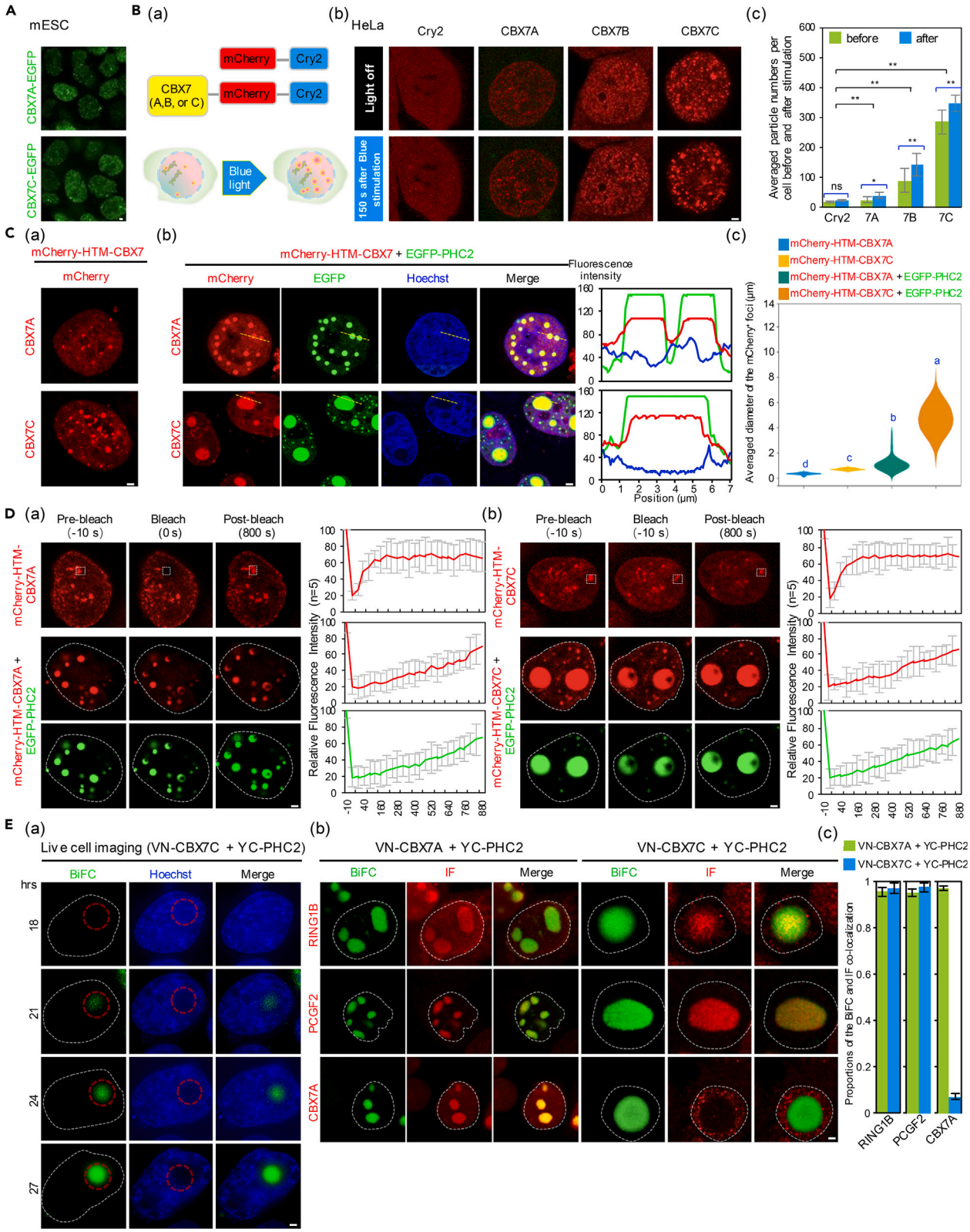
A
mESC
CBX7A-EGFP
CBX7C-EGFP
B (a)
CBX7 (A,B, or C)
mCherry
Cry2
Blue light
(b)
HeLa
Cry2
CBX7A
CBX7B
CBX7C
Light off
150 s after Blue stimulation
(c)
Averaged particle numbers per cell before and after stimulation
before
after
ns
Cry2
7A
7B
7C
C (a)
mCherry-HTM-CBX7
mCherry
CBX7A
CBX7C
(b)
mCherry-HTM-CBX7 + EGFP-PHC2
mCherry
EGFP
Hoechst
Merge
Fluorescence intensity
Position (μm)
(c)
mCherry-HTM-CBX7A
mCherry-HTM-CBX7C
mCherry-HTM-CBX7A +EGFP-PHC2
mCherry-HTM-CBX7C + EGFP-PHC2
Averaged diameter of the mCherry foci (μm)
D (a)
Pre-bleach (-10 s)
Bleach (0 s)
Post-bleach (800 s)
mCherry-HTM-CBX7A
mCherry-HTM-CBX7A + EGFP-PHC2
Relative Fluorescence Intensity (n=5)
(b)
Pre-bleach (-10 s)
Bleach (-10 s)
Post-bleach (800 s)
mCherry-HTM-CBX7C
mCherry-HTM-CBX7C + EGFP-PHC2
Relative Fluorescence Intensity (n=5)
E (a)
Live cell imaging (VN-CBX7C + YC-PHC2)
BiFC
Hoechst
Merge
hrs
18
21
24
27
(b)
VN-CBX7A + YC-PHC2
VN-CBX7C + YC-PHC2
BiFC
IF
Merge
RING1B
PCGF2
CBX7A
(c)
VN-CBX7A + YC-PHC2
VN-CBX7C + YC-PHC2
Proportions of the BiFC and IF co-localization
RING1B
PCGF2
CBX7A

Figure 5. Comparison of the phase separation capability of the CBX7 isoforms

(A) Confocal images of the mESC stable cell line expressing CBX7A or CBX7C. Scale bar, 2 μm.

(B) Detection of the LLPS properties of the three CBX7 isoforms via an optogenetic platform expressing one of the CBX7 isoform fused to Cry2 and mCherry. The simplified scheme of the optogenetic system is shown in (a), and the confocal images of the cells before and after blue light activation are shown in (b). Scale bar, 2 μm. Particle numbers were measured using ImageJ software. All error bars represent the standard error of the mean numbers from 3 cells for each condition, and the significant differences between means were determined using Student's t test (*$p < 0.05$; **$p < 0.01$; ns, not significant, $p > 0.05$) (c). Data are represented as mean ± SD.

(C) The confocal images of HeLa cells transiently transfected with mCherry-HTM-CBX7A or CBX7C alone (a) or together with EGFP-PHC2 (b). Scale bar stands for 2 μm in (a) and 4 μm in (b). Chromatin was labeled via Hoechst staining. The intensity of various fluorescence across the randomly selected regions (shown as the dashed lines) was scanned and plotted on the right of each image to demonstrate the colocalization status of the indicated factors or modifications. (the right part of b). The diameter of mCherry positive foci was measured using ImageJ software (c). The letters marked indicate significant differences as determined using ANOVA followed by Duncan's multiple range test ($p < 0.05$).

(D) FRAP analyses monitoring the dynamic diffusion properties of the various types of foci formed in (C). Each of the marked region was bleached with a 488-nm laser pulse at time 0. The line charts on the right demonstrate the relative changes of the fluorescence intensities of each marked region at the indicated time points before and after the photobleaching. Scale bar, 2 μm.

(E) Live cell detection of the dynamic formation process of the CBX7C•PHC2 BiFC condensates using DeltaVision Elite high-resolution live cell imaging system (a) and analyses of their composition (b). The images shown were taken every 3 h starting from 18 h post transfection (a). Detection of the endogenous PRC1 components in the CBX7•PHC2 BiFC condensates via IF assays (b). Scale bars, 2 μm. A bar graph indicates the proportions of the colocalized foci (BiFC and the indicated IF signals) to the total BiFC positive foci shown in E(c), quantified by ImageJ. Data are represented as mean ± SD. Nucleus outlines are indicated with dashed lines in (D and E).

It turned out the loss of SAM only slightly affected the interaction between CBX7A or CBX7C and PHC2 (Figure 6A), indicating that the SAM domain was not essential for their direct interaction.

To further identify the key region(s) responsible for the CBX7•PHC2-coordinated phase separation, we employed BiFC assays and tested the condensate formed by the full length or the truncated forms of the abovementioned factors (Figure 6B). The results indicated that either the N- or the C-termini of CBX7A and CBX7C were sufficient to undergo phase separation together with PHC2. However, compared with the full-length counterpart, the extent of CBX7•PHC2-mediated phase separation was greatly discounted upon the deletion of SAM in PHC2, with a significant amount of the BiFC signals diffused throughout the nucleus (Figure 6B). Interestingly, notable differences were observed between the N- and C-termini of the CBX7 isoforms. The vast majority of the condensates formed by the N-terminus of CBX7A or CBX7C with $PHC2_{\Delta SAM}$ were partially colocalized with the compact chromatin with their sizes similar to the regular Pc bodies observed (Figure 6B). In the case of the $CBX7C_C$•$PHC2_{\Delta SAM}$ interaction, they also formed much smaller condensates than the ones made by their full-length counterparts. Importantly, these condensates partially colocalized with the H2AK119ub mark, therefore representing the functional Pc bodies (Figure 6C). In contrast, the C-terminus of CBX7A or CBX7C with $PHC2_{\Delta SAM}$ remained to form the huge condensates with chromatin being excluded. These results indicated that the N-terminus of CBX7 played a crucial role in chromatin targeting and formation of enzymatically active cPRC1, whereas the SAM domain of PHC2 significantly affected the coordinated phase separation of the chromatin-free CBX7•PHC2 condensates. Furthermore, the C-terminus of CBX7C played a more important role than CBX7A in the phase separation process of generating chromatin-free condensates, which well explained the differential phase separation capabilities between CBX7C and CBX7A seen earlier. Taken together, the whole set of data supports a model that the CBX7•PHC2-mediated Pc body formation might be a self-controllable phase transition event with distinct outcomes. When the core factors are expressed at low or modest doses, the initial formation of the functional Pc bodies is a process of LLPS mainly achieved by the intermolecular interactions between the N-terminus of CBX7C and PHC2. In the case of highly expressing both components, the phase transition into the dysfunctional, chromatin-free condensates is promoted, which relies on the further contribution of both the C-terminus of CBX7C and the SAM domain of PHC2.

DISCUSSION

In this study, we investigate the functional properties of an uncharacterized *Cbx7* splicing isoform, *Cbx7C*, which is lacking the C-terminal PC domain. Our data discover that CBX7C is specifically expressed in mESCs and utilizes a unique PRC1 assembly strategy. In this model, PHC2 is alternatively serving as a bridging molecule in between RING1B and CBX7, and the CBX7C•PHC2 dimer may be set a core to facilitate the *in situ* assembly of cPRC1 on chromatin (Figure 7). Furthermore, the cPRC1 complexes bound at various targets gather together to form Pc bodies through LLPS to achieve more effective transcriptional corepression. Therefore, CBX7C may play an important role as a potent cPRC1 organizer to drive the establishment of the epigenetic repressive function, rather than acting as an independent regulator as another PC-less CBX2 isoform.[21] This indicates that the emergence of distinct splicing isoforms of the cPRC1 components during evolution may greatly increase the diversity and the sophisticated division of PRC1.

Our results demonstrate that the phase separation potential of CBX7C is greater than CBX7A and further enhanced upon the interaction to PHC2. CBX7C alone was sufficient to form condensates via LLPS in cells. Although PHC2 binds to DNA *in vitro*, the purified PHC proteins can only form condensates along with the chromatin templates.[32] Therefore, PHC2 possibly relies on the other PRC1 components or transcription factors to achieve its enrichment at certain target genes.[30,31,57–59] In addition, it is known that the PHC proteins mainly exist as oligomers through the head-to-tail connection of the SAM domain.[29,60–62] Based on all these findings, CBX7C may act as an initiator for target recognition and cPRC1 assembly, whereas further inclusion of PHC2 greatly enhances the formation of Pc bodies (Figure 7).

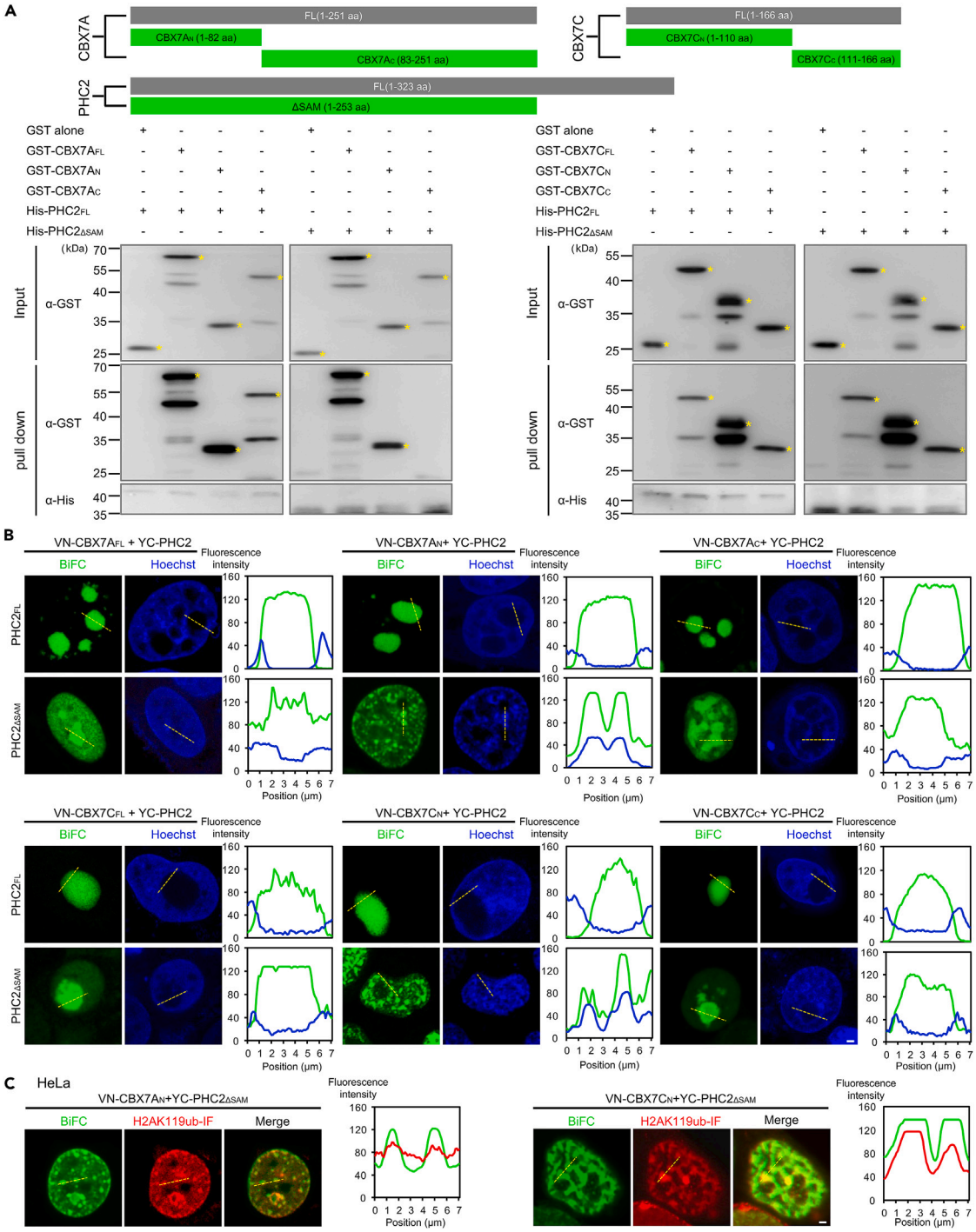

Figure 6. Identification of the domains/regions involved in the CBX7●PHC2 interaction and their coordinated phase separation

(A) His pull-down analyses between PHC2 and the full length (FL) or the truncated forms of CBX7 isoforms. The subscripts N or C stands for the N- or C-terminus of the indicated CBX7 isoform. The asterisk indicates the positions of the intact proteins with GST-tag.

(B) Analyses of the phase separation properties in HeLa cells transfected with the indicated BiFC plasmid pairs. The measurement of the fluorescent intensity was carried out as described in Figure 3D.

(C) The confocal images of IF assays detecting the distribution of the H2AK119ub in the foci generated by the indicated forms of CBX7 and PHC2. Scale bars (B and C), 2 μm.

Some recent reports proposed a client-scaffold model in which CBX2 was modestly expressed in mESCs and acted as a scaffold based on its intrinsic properties and its interactions to the other phase separation-prone PRC1 subunits.[15,63] Our data suggest that CBX7C may supplement or even replace the function of CBX7A and CBX7B in mESCs during differentiation. We propose that CBX7C works as a seeding factor to initiate complex assembly and further amplify its valence to drive the formation of larger condensates under the assistance of PHC2. Certainly, future efforts should be directed toward understanding the biological functions of CBX7C under the corresponding physiological scenarios.

In this study, the intrinsic properties of the CBX7C•PHC2 condensates are found varied according to their cellular doses. At normal concentration, the catalytically active Pc bodies are formed, whereas when the doses are higher than the threshold, the condensates tend to undergo the liquid-solid phase transition and converge into a dense hydrogel with the chromatin being excluded simultaneously. At the same time, the dense condensates continuously absorb PRC1 components from the cellular pool like a molecular sponge. Because the chromatic modifying enzymes are spatially encapsulated in these condensates, isolated from their histone targets, the resultant Pc bodies are virtually dysfunctional even with all the components included. Our systematic analyses of the truncation mutants help dissect the detailed process of these phase separation events. The SAM domain of PHC2 is not required for the direct interaction to CBX7C, whereas it helps strengthen the formation of the hydrogel aggregates. The N-terminus of CBX7C mainly mediates the dimer formation of CBX7C•PHC2 and is sufficient to drive the generation of the enzymatically active Pc bodies via LLPS in the absence of SAM. However, the C-terminus of CBX7C mainly plays a role in promoting the formation of the CBX7C•PHC2 aggregates with hydrogel properties, which is possibly associated with the development of diseases (Figure 7). Overall, the conformation of CBX7C•PHC2 interaction may play an essential role in defining the involved domains and thus determine the choice of phase separation.

Taken together, this study uncovers that various CBX7 isoforms have distinct properties and working mechanisms in complex assembly and Pc body formation, emphasizing the essential role of CBX7C in mESC differentiation. The main finding of this study provides a promising strategy of regulating the homeostasis of cellular PRC1 activities via the modulation of its phase separation capabilities.

Limitations of the study

In this study, although the expression level of *Cbx7C* detected in mESCs was relatively low, we observed severe differentiation defects during the ESC to EB process upon knocking down of *Cbx7C*. However, the poor growth status of these knockdown cells aborted the effective sample collection and following analyses. Thus, alternative strategies such as conditional knockdown via RNAi or inducible degron system would be useful in the future to uncover CBX7C's essential functions and its relationship with the other CBX7 isoforms during differentiation.

In addition, although the combination of the methodologies used in this study was efficient to support our main conclusions about the phase separation properties of CBX7 isoforms, more direct evidence obtained under physiological conditions remains needed in order to reveal the delicate mechanisms of how distinct CBX7 isoforms trigger LLPS and/or other types of phase separation differently. Another related limitation was that we only tested the short form of PHC2 (323 aa), which contained the three conserved domains, HD1, FCS zinc finger, and SAM, and had been used as a classical model to the study of its phase separation and SAM-mediated polymerization.[32,64] The CBX7·PHC2 interaction with the long form of PHC2 (850 aa) remains to be further explored.

STAR★METHODS

Detailed methods are provided in the online version of this paper and include the following:

- KEY RESOURCES TABLE
- RESOURCE AVAILABILITY
  - Lead contact
  - Materials availability
  - Data and code availability
- EXPERIMENTAL MODEL AND STUDY PARTICIPANT DETAILS
  - Cell culture
- METHOD DETAILS
  - shRNA-mediated knockdown
  - Generation of stable cell lines
  - BiFC assays
  - Pull-down assays
  - Production of CBX7C polyclonal antibody
  - Co-immunoprecipitation assays
  - Chromatin immunoprecipitation and qPCR assays
  - Fluorescence recovery after photo bleaching (FRAP)
  - Embryoid bodies preparation assays
  - Quantitative real-time PCR
  - Immunofluorescence assays

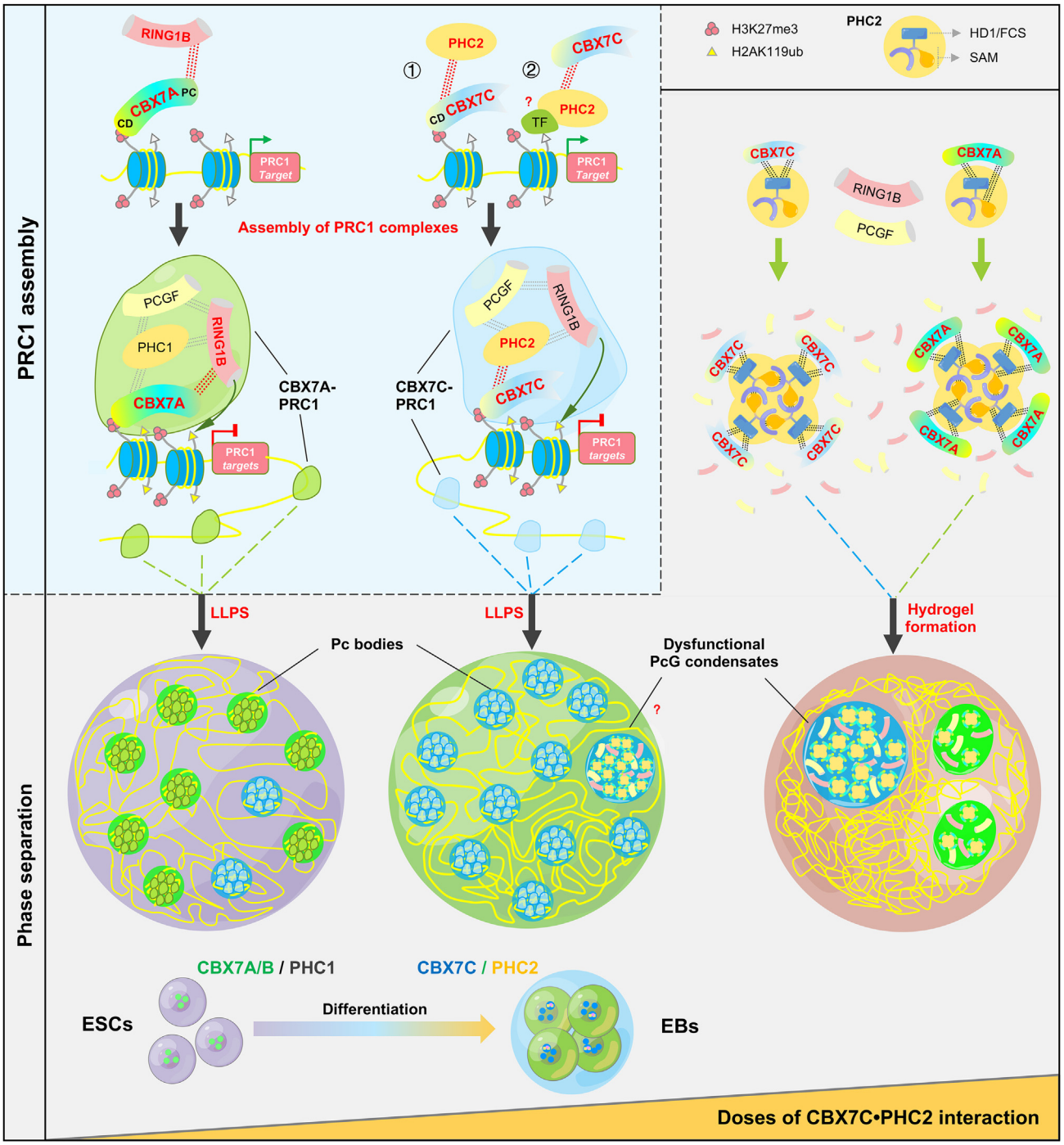

Figure 7. A working model of CBX7C and 7A in participating PRC1 assembly and phase separation in mESCs and during differentiation

The switch of PRC1 components and their isoforms during the differentiation of mESCs modulate the composition of PRC1. The cellular levels of CBX7C•PHC2 interaction strongly affect the phase separation properties and the functions of PRC1.

- Reporter assays
- QUANTIFICATION AND STATISTICAL ANALYSES

SUPPLEMENTAL INFORMATION

Supplemental information can be found online at https://doi.org/10.1016/j.isci.2024.109548.

ACKNOWLEDGMENTS

This work was financially supported by the National Natural Science Foundation of China (31471233, 31771447, 31970624 to Bo Cheng), the Foundation of the Ministry of Education Key Laboratory of Cell Activities and Stress Adaptations grant (lzujbky-2021-kb05 to Bo Cheng), a research project sponsored by Agilent (ACT-UR #4772 to Bo Cheng), the Fundamental Research Funds for the Central Universities (lzujbky-2022-ct05 to Bo Cheng), and the Gansu Provincial Outstanding Graduate Student Project (22JR5RA42 to Shanli Guan). We also thank the core facilities in the School of Life Sciences, Lanzhou University for providing high-quality instruments and service for our confocal microscopy experiments.

AUTHOR CONTRIBUTIONS

S.G. performed experiments, analyzed the data, and designed the figures together with J.T. and X.M. S.G. and B.C. wrote the manuscript. R.M. and B.C. supervised and conceived the project. All the authors read and approved the final manuscript.

DECLARATION OF INTERESTS

The authors have no conflicts of interest to declare.

Received: August 6, 2023
Revised: February 4, 2024
Accepted: March 19, 2024
Published: March 21, 2024

REFERENCES

1. Völkel, P., and Angrand, P.O. (2007). The control of histone lysine methylation in epigenetic regulation. Biochimie *89*, 1–20. https://doi.org/10.1016/j.biochi.2006.07.009.
2. Schwartz, Y.B., and Pirrotta, V. (2008). Polycomb complexes and epigenetic states. Curr. Opin. Cell Biol. *20*, 266–273. https://doi.org/10.1016/j.ceb.2008.03.002.
3. Bernstein, E., Duncan, E.M., Masui, O., Gil, J., Heard, E., and Allis, C.D. (2006). Mouse polycomb proteins bind differentially to methylated histone H3 and RNA and are enriched in facultative heterochromatin. Mol. Cell Biol. *26*, 2560–2569. https://doi.org/10.1128/Mcb.26.7.2560-2569.2006.
4. de Napoles, M., Mermoud, J.E., Wakao, R., Tang, Y.A., Endoh, M., Appanah, R., Nesterova, T.B., Silva, J., Otte, A.P., Vidal, M., et al. (2004). Polycomb group proteins Ring1A/B link ubiquitylation of histone H2A to heritable gene silencing and X inactivation. Dev. Cell *7*, 663–676. https://doi.org/10.1016/j.devcel.2004.10.005.
5. Fioriniello, S., Marano, D., Fiorillo, F., D'Esposito, M., and Della Ragione, F. (2020). Epigenetic Factors that Control Pericentric Heterochromatin Organization in Mammals. Genes-Basel *11*, 595. https://doi.org/10.3390/genes11060595.
6. Blackledge, N.P., Rose, N.R., and Klose, R.J. (2015). Targeting Polycomb systems to regulate gene expression: modifications to a complex story. Nat. Rev. Mol. Cell Biol. *16*, 643–649. https://doi.org/10.1038/nrm4067.
7. Aranda, S., Mas, G., and Di Croce, L. (2015). Regulation of gene transcription by Polycomb proteins. Sci. Adv. *1*, e1500737. https://doi.org/10.1126/sciadv.1500737.
8. Schwartz, Y.B., and Pirrotta, V. (2014). Ruled by Ubiquitylation: A New Order for Polycomb Recruitment. Cell Rep. *8*, 321–325. https://doi.org/10.1016/j.celrep.2014.07.001.
9. Gao, Z., Zhang, J., Bonasio, R., Strino, F., Sawai, A., Parisi, F., Kluger, Y., and Reinberg, D. (2012). PCGF Homologs, CBX Proteins, and RYBP Define Functionally Distinct PRC1 Family Complexes. Mol. Cell *45*, 344–356. https://doi.org/10.1016/j.molcel.2012.01.002.
10. Tavares, L., Dimitrova, E., Oxley, D., Webster, J., Poot, R., Demmers, J., Bezstarosti, K., Taylor, S., Ura, H., Koide, H., et al. (2012). RYBP-PRC1 complexes mediate H2A ubiquitylation at polycomb target sites independently of PRC2 and H3K27me3. Cell *148*, 664–678. https://doi.org/10.1016/j.cell.2011.12.029.
11. Cao, R., Wang, L., Wang, H., Xia, L., Erdjument-Bromage, H., Tempst, P., Jones, R.S., and Zhang, Y. (2002). Role of histone H3 lysine 27 methylation in polycomb-group silencing. Science *298*, 1039–1043. https://doi.org/10.1126/science.1076997.
12. Min, J., Zhang, Y., and Xu, R.M. (2003). Structural basis for specific binding of polycomb chromodomain to histone H3 methylated at Lys 27. Gene Dev. *17*, 1823–1828. https://doi.org/10.1101/gad.269603.
13. Kaustov, L., Ouyang, H., Amaya, M., Lemak, A., Nady, N., Duan, S., Wasney, G.A., Li, Z., Vedadi, M., Schapira, M., et al. (2011). Recognition and Specificity Determinants of the Human Cbx Chromodomains. J. Biol. Chem. *286*, 521–529. https://doi.org/10.1074/jbc.M110.191411.
14. Fischle, W., Wang, Y., Jacobs, S.A., Kim, Y., Allis, C.D., and Khorasanizadeh, S. (2003). Molecular basis for the discrimination of repressive methyl-lysine marks in histone H3 by Polycomb and HP1 chromodomains. Gene Dev. *17*, 1870–1881. https://doi.org/10.1101/gad.1110503.
15. Kent, S., Brown, K., Yang, C.H., Alsaihati, N., Tian, C., Wang, H., and Ren, X. (2020). Phase-Separated Transcriptional Condensates Accelerate Target-Search Process Revealed by Live-Cell Single-Molecule Imaging. Cell Rep. *33*, 108248. https://doi.org/10.1016/j.celrep.2020.108248.
16. Eeftens, J.M., Kapoor, M., Michieletto, D., and Brangwynne, C.P. (2021). Polycomb condensates can promote epigenetic marks but are not required for sustained chromatin compaction. Nat. Commun. *12*, 5888. https://doi.org/10.1038/s41467-021-26147-5.
17. Bezsonova, I., Walker, J.R., Bacik, J.P., Duan, S., Dhe-Paganon, S., and Arrowsmith, C.H. (2009). Ring1B contains a ubiquitin-like docking module for interaction with Cbx proteins. Biochemistry *48*, 10542–10548. https://doi.org/10.1021/bi901131u.
18. Wang, R., Taylor, A.B., Leal, B.Z., Chadwell, L.V., Ilangovan, U., Robinson, A.K., Schirf, V., Hart, P.J., Lafer, E.M., Demeler, B., et al. (2010). Polycomb Group Targeting through Different Binding Partners of RING1B C-Terminal Domain. Structure *18*, 966–975. https://doi.org/10.1016/j.str.2010.04.013.
19. Vincenz, C., and Kerppola, T.K. (2008). Different polycomb group CBX family proteins associate with distinct regions of chromatin using nonhomologous protein sequences. Proc. Natl. Acad. Sci. USA *105*, 16572–16577. https://doi.org/10.1073/pnas.0805317105.
20. Glancy, E., Wang, C., Tuck, E., Healy, E., Amato, S., Neikes, H.K., Mariani, A., Mucha, M., Vermeulen, M., Pasini, D., and Bracken, A.P. (2023). PRC2.1- and PRC2.2-specific accessory proteins drive recruitment of different forms of canonical PRC1. Mol. Cell *83*, 1393–1411.e7. https://doi.org/10.1016/j.molcel.2023.03.018.
21. Völkel, P., Le Faou, P., Vandamme, J., Pira, D., and Angrand, P.O. (2012). A human Polycomb isoform lacking the Pc box does not participate to PRC1 complexes but forms protein assemblies and represses transcription. Epigenetics *7*, 482–491. https://doi.org/10.4161/epi.19741.
22. Le Faou, P., Völkel, P., and Angrand, P.O. (2011). The zebrafish genes encoding the Polycomb repressive complex (PRC) 1. Gene *475*, 10–21. https://doi.org/10.1016/j.gene.2010.12.012.
23. Satijn, D.P., Olson, D.J., vanderVlag, J., Hamer, K.M., Lambrechts, C., Masselink, H., Gunster, M.J., Sewalt, R.G., vanDriel, R., and Otte, A.P. (1997). Interference with the expression of a novel human polycomb

protein, hPc2, results in cellular transformation and apoptosis. Mol. Cell Biol. *17*, 6076–6086. https://doi.org/10.1128/Mcb.17.10.6076.

24. Francis, N.J., Kingston, R.E., and Woodcock, C.L. (2004). Chromatin compaction by a polycomb group protein complex. Science *306*, 1574–1577. https://doi.org/10.1126/science.1100576.
25. Eskeland, R., Leeb, M., Grimes, G.R., Kress, C., Boyle, S., Sproul, D., Gilbert, N., Fan, Y., Skoultchi, A.I., Wutz, A., and Bickmore, W.A. (2010). Ring1B Compacts Chromatin Structure and Represses Gene Expression Independent of Histone Ubiquitination. Mol. Cell *38*, 452–464. https://doi.org/10.1016/j.molcel.2010.02.032.
26. Tatavosian, R., Kent, S., Brown, K., Yao, T., Duc, H.N., Huynh, T.N., Zhen, C.Y., Ma, B., Wang, H., and Ren, X. (2019). Nuclear condensates of the Polycomb protein chromobox 2 (CBX2) assemble through phase separation. J. Biol. Chem. *294*, 1451–1463. https://doi.org/10.1074/jbc.RA118.006620.
27. Plys, A.J., Davis, C.P., Kim, J., Rizki, G., Keenen, M.M., Marr, S.K., and Kingston, R.E. (2019). Phase separation of Polycomb-repressive complex 1 is governed by a charged disordered region of CBX2. Gene Dev. *33*, 799–813. https://doi.org/10.1101/gad.326488.119.
28. Cheutin, T., and Cavalli, G. (2018). Loss of PRC1 induces higher-order opening of Hox loci independently of transcription during Drosophila embryogenesis. Nat. Commun. *9*, 3898. https://doi.org/10.1038/s41467-018-05945-4.
29. Kim, C.A., Gingery, M., Pilpa, R.M., and Bowie, J.U. (2002). The SAM domain of polyhomeotic forms a helical polymer. Nat. Struct. Biol. *9*, 453–457. https://doi.org/10.1038/nsb802.
30. Robinson, A.K., Leal, B.Z., Chadwell, L.V., Wang, R., Ilangovan, U., Kaur, Y., Junco, S.E., Schirf, V., Osmulski, P.A., Gaczynska, M., et al. (2012). The Growth-Suppressive Function of the Polycomb Group Protein Polyhomeotic Is Mediated by Polymerization of Its Sterile Alpha Motif (SAM) Domain. J. Biol. Chem. *287*, 8702–8713. https://doi.org/10.1074/jbc.M111.336115.
31. Isono, K., Endo, T.A., Ku, M., Yamada, D., Suzuki, R., Sharif, J., Ishikura, T., Toyoda, T., Bernstein, B.E., and Koseki, H. (2013). SAM Domain Polymerization Links Subnuclear Clustering of PRC1 to Gene Silencing. Dev. Cell *26*, 565–577. https://doi.org/10.1016/j.devcel.2013.08.016.
32. Seif, E., Kang, J.J., Sasseville, C., Senkovich, O., Kaltashov, A., Boulier, E.L., Kapur, I., Kim, C.A., and Francis, N.J. (2020). Phase separation by the polyhomeotic sterile alpha motif compartmentalizes Polycomb Group proteins and enhances their activity. Nat. Commun. *11*, 5609. https://doi.org/10.1038/s41467-020-19435-z.
33. Kapur, I., Boulier, E.L., and Francis, N.J. (2022). Regulation of Polyhomeotic Condensates by Intrinsically Disordered Sequences That Affect Chromatin Binding. Epigenomes *6*, 40. https://doi.org/10.3390/epigenomes6040040.
34. Jaensch, E.S., Zhu, J., Cochrane, J.C., Marr, S.K., Oei, T.A., Damle, M., McCaslin, E.Z., and Kingston, R.E. (2021). A Polycomb domain found in committed cells impairs differentiation when introduced into PRC1 in pluripotent cells. Mol. Cell *81*, 4677–4691.e8. https://doi.org/10.1016/j.molcel.2021.09.018.
35. Brown, K., Chew, P.Y., Ingersoll, S., Espinosa, J.R., Aguirre, A., Espinoza, A., Wen, J., Astatike, K., Kutateladze, T.G., Collepardo-Guevara, R., and Ren, X. (2023). Principles of assembly and regulation of condensates of Polycomb repressive complex 1 through phase separation. Cell Rep. *42*, 113136. https://doi.org/10.1016/j.celrep.2023.113136.
36. Wei, C., Jia, L., Huang, X., Tan, J., Wang, M., Niu, J., Hou, Y., Sun, J., Zeng, P., Wang, J., et al. (2022). CTCF organizes inter-A compartment interactions through RYBP-dependent phase separation. Cell Res. *32*, 744–760. https://doi.org/10.1038/s41422-022-00676-0.
37. Liu, X., Jiang, S., Ma, L., Qu, J., Zhao, L., Zhu, X., and Ding, J. (2021). Time-dependent effect of 1,6-hexanediol on biomolecular condensates and 3D chromatin organization. Genome Biol. *22*, 230. https://doi.org/10.1186/s13059-021-02455-3.
38. Morey, L., Pascual, G., Cozzuto, L., Roma, G., Wutz, A., Benitah, S.A., and Di Croce, L. (2012). Nonoverlapping Functions of the Polycomb Group Cbx Family of Proteins in Embryonic Stem Cells. Cell Stem Cell *10*, 47–62. https://doi.org/10.1016/j.stem.2011.12.006.
39. Gray, F., Cho, H.J., Shukla, S., He, S., Harris, A., Boytsov, B., Jaremko, Ł., Jaremko, M., Demeler, B., Lawlor, E.R., et al. (2016). BMI1 regulates PRC1 architecture and activity through homo- and hetero-oligomerization. Nat. Commun. *7*, 13343. https://doi.org/10.1038/ncomms13343.
40. Chen, L., Tong, Q., Chen, X., Jiang, P., Yu, H., Zhao, Q., Sun, L., Liu, C., Gu, B., Zheng, Y., et al. (2021). PHC1 maintains pluripotency by organizing genome-wide chromatin interactions of the Nanog locus. Nat. Commun. *12*, 2829. https://doi.org/10.1038/s41467-021-22871-0.
41. Isono, K.I., Fujimura, Y.I., Shinga, J., Yamaki, M., O-Wang, J., Takihara, Y., Murahashi, Y., Takada, Y., Mizutani-Koseki, Y., and Koseki, H. (2005). Mammalian polyhomeotic homologues Phc2 and Phc1 act in synergy to mediate polycomb repression of Hox genes. Mol. Cell Biol. *25*, 6694–6706. https://doi.org/10.1128/MCB.25.15.6694-6706.2005.
42. Souza, P.P., Völkel, P., Trinel, D., Vandamme, J., Rosnoblet, C., Héliot, L., and Angrand, P.O. (2009). The histone methyltransferase SUV420H2 and Heterochromatin Proteins HP1 interact but show different dynamic behaviours. BMC Cell Biol. *10*, 41. https://doi.org/10.1186/1471-2121-10-41.
43. Zhao, J., Wang, M., Chang, L., Yu, J., Song, A., Liu, C., Huang, W., Zhang, T., Wu, X., Shen, X., et al. (2020). RYBP/YAF2-PRC1 complexes and histone H1-dependent chromatin compaction mediate propagation of H2AK119ub1 during cell division. Nat. Cell Biol. *22*, 439–452. https://doi.org/10.1038/s41556-020-0484-1.
44. O'Loghlen, A., Muñoz-Cabello, A.M., Gaspar-Maia, A., Wu, H.A., Banito, A., Kunowska, N., Racek, T., Pemberton, H.N., Beolchi, P., Lavial, F., et al. (2012). MicroRNA Regulation of Cbx7 Mediates a Switch of Polycomb Orthologs during ESC Differentiation. Cell Stem Cell *10*, 33–46. https://doi.org/10.1016/j.stem.2011.12.004.
45. Cheutin, T., and Cavalli, G. (2012). Progressive Polycomb Assembly on H3K27me3 Compartments Generates Polycomb Bodies with Developmentally Regulated Motion. PLoS Genet. *8*, e1002465. https://doi.org/10.1371/journal.pgen.1002465.
46. Grimaud, C., Bantignies, F., Pal-Bhadra, M., Ghana, P., Bhadra, U., and Cavalli, G. (2006). RNAi components are required for nuclear clustering of Polycomb group response elements. Cell *124*, 957–971. https://doi.org/10.1016/j.cell.2006.01.036.
47. Buchenau, P., Hodgson, J., Strutt, H., and Arndt-Jovin, D.J. (1998). The distribution of polycomb-group proteins during cell division and development in Drosophila embryos: impact on models for silencing. J. Cell Biol. *141*, 469–481. https://doi.org/10.1083/jcb.141.2.469.
48. Messmer, S., Franke, A., and Paro, R. (1992). Analysis of the functional role of the Polycomb chromo domain in Drosophila melanogaster. Gene Dev. *6*, 1241–1254. https://doi.org/10.1101/gad.6.7.1241.
49. Banani, S.F., Lee, H.O., Hyman, A.A., and Rosen, M.K. (2017). Biomolecular condensates: organizers of cellular biochemistry. Nat. Rev. Mol. Cell Biol. *18*, 285–298. https://doi.org/10.1038/nrm.2017.7.
50. Brangwynne, C., Tompa, P., and Pappu, R. (2015). Polymer physics of intracellular phase transitions. Nat. Phys. *11*, 899–904. https://doi.org/10.1038/Nphys3532.
51. Nott, T.J., Petsalaki, E., Farber, P., Jervis, D., Fussner, E., Plochowietz, A., Craggs, T.D., Bazett-Jones, D.P., Pawson, T., Forman-Kay, J.D., and Baldwin, A.J. (2015). Phase Transition of a Disordered Nuage Protein Generates Environmentally Responsive Membraneless Organelles. Mol. Cell *57*, 936–947. https://doi.org/10.1016/j.molcel.2015.01.013.
52. Shin, Y., and Brangwynne, C.P. (2017). Liquid phase condensation in cell physiology and disease. Science *357*, eaaf4382. https://doi.org/10.1126/science.aaf4382.
53. Shin, Y., Berry, J., Pannucci, N., Haataja, M.P., Toettcher, J.E., and Brangwynne, C.P. (2017). Spatiotemporal Control of Intracellular Phase Transitions Using Light-Activated optoDroplets. Cell *168*, 159–171.e14. https://doi.org/10.1016/j.cell.2016.11.054.
54. Cho, K.W., Andrade, M., Zhang, Y., and Yoon, Y.S. (2020). Mammalian CBX7 isoforms p36 and p22 exhibit differential responses to serum, varying functions for proliferation, and distinct subcellular localization. Sci. Rep. *10*, 8061. https://doi.org/10.1038/s41598-020-64908-2.
55. Alberti, S., Gladfelter, A., and Mittag, T. (2019). Considerations and Challenges in Studying Liquid-Liquid Phase Separation and Biomolecular Condensates. Cell *176*, 419–434. https://doi.org/10.1016/j.cell.2018.12.035.
56. Harmon, T.S., Holehouse, A.S., Rosen, M.K., and Pappu, R.V. (2017). Intrinsically disordered linkers determine the interplay between phase separation and gelation in multivalent proteins. Elife *6*, e30294. https://doi.org/10.7554/eLife.30294.
57. Wani, A.H., Boettiger, A.N., Schorderet, P., Ergun, A., Münger, C., Sadreyev, R.I., Zhuang, X., Kingston, R.E., and Francis, N.J. (2016). Chromatin topology is coupled to Polycomb group protein subnuclear organization. Nat. Commun. *7*, 10291. https://doi.org/10.1038/ncomms10291.
58. Gambetta, M.C., and Müller, J. (2014). O-GlcNAcylation prevents aggregation of the Polycomb group repressor polyhomeotic.

Dev. Cell *31*, 629–639. https://doi.org/10.1016/j.devcel.2014.10.020.

59. Tsuboi, M., Kishi, Y., Yokozeki, W., Koseki, H., Hirabayashi, Y., and Gotoh, Y. (2018). Ubiquitination-Independent Repression of PRC1 Targets during Neuronal Fate Restriction in the Developing Mouse Neocortex. Dev. Cell *47*, 758–772.e5. https://doi.org/10.1016/j.devcel.2018.11.018.
60. Loubiere, V., Martinez, A.M., and Cavalli, G. (2019). Cell Fate and Developmental Regulation Dynamics by Polycomb Proteins and 3D Genome Architecture. Bioessays *41*, e1800222. https://doi.org/10.1002/bies.201800222.
61. Kim, C.A., and Bowie, J.U. (2003). SAM domains: uniform structure, diversity of function. Trends Biochem. Sci. *28*, 625–628. https://doi.org/10.1016/j.tibs.2003.11.001.
62. Robinson, A.K., Leal, B.Z., Nanyes, D.R., Kaur, Y., Ilangovan, U., Schirf, V., Hinck, A.P., Demeler, B., and Kim, C.A. (2012). Human polyhomeotic homolog 3 (PHC3) sterile alpha motif (SAM) linker allows open-ended polymerization of PHC3 SAM. Biochemistry *51*, 5379–5386. https://doi.org/10.1021/bi3004318.
63. Tatavosian, R., Duc, H.N., Huynh, T.N., Fang, D., Schmitt, B., Shi, X., Deng, Y., Phiel, C., Yao, T., Zhang, Z., et al. (2018). Live-cell single-molecule dynamics of PcG proteins imposed by the DIPG H3.3K27M mutation. Nat. Commun. *9*, 2080. https://doi.org/10.1038/s41467-018-04455-7.
64. Robinson, A.K., Leal, B.Z., Chadwell, L.V., Wang, R., Ilangovan, U., Kaur, Y., Junco, S.E., Schirf, V., Osmulski, P.A., Gaczynska, M., et al. (2012). The growth-suppressive function of the polycomb group protein polyhomeotic is mediated by polymerization of its sterile alpha motif (SAM) domain. J. Biol. Chem. *287*, 8702–8713. https://doi.org/10.1074/jbc.M111.336115.
65. Cheng, B., Li, T., Rahl, P.B., Adamson, T.E., Loudas, N.B., Guo, J., Varzavand, K., Cooper, J.J., Hu, X., Gnatt, A., et al. (2012). Functional Association of Gdown1 with RNA Polymerase II Poised on Human Genes. Mol. Cell *45*, 38–50. https://doi.org/10.1016/j.molcel.2011.10.022.

STAR★METHODS

KEY RESOURCES TABLE

REAGENT or RESOURCE	SOURCE	IDENTIFIER
Antibodies		
Rabbit ant CBX7C	This paper	N/A
Mouse anti His	Abmart	Cat#M30111 RRID: AB_2889874
Mouse anti GST	Abmart	Cat#M20007; RRID: AB_2864360
Mouse anti Flag	Abmart	Cat#M20008; RRID: AB_2713960
Rabbit anti RING1B	CST	Cat#5694; RRID: AB_10705604
Rabbit anti CBX7	Abcam	Cat#ab21873; RRID: AB_726005
Rabbit anti PCGF2	Abclonal	Cat#A17327; RRID: AB_2770811
Rabbit anti H3K27me3	PTM BIO	Cat#PTM-622; RRID: AB_2752230
Rabbit anti H2AK119ub	CST	Cat#8240; RRID: AB_10891618
Goat-*anti*-Rabbit IgG/Alexa Fluor 594	Abcam	Cat#ab150116; RRID: AB_2650601
Bacterial and virus strains		
pLKO-*Cbx7C* shRNA #1-3-Puro	This paper	N/A
Biological samples		
Healthy adult C57BL/6 mouse	Medical Experimental Center of Lanzhou University	N/A
Chemicals, peptides, and recombinant proteins		
Doxycycline	Biogems	2431450
G418	Sangon Biotech	A100859
Hoechst 33342	Solarbio Life Sciences	C0031
Critical commercial assays		
BeaverBeads™ GSH	Beaver	70601
BeaverBeads™ IDA-Co	Beaver	70502
GE-CNBr activated Sepharose™ 4B	GE Healthcare	71-7086-00
Protein A/G magnetic beads	Beaver	22202
RNaseA	TransGen Biotech	RL4250
Protease K	ThermoFisher	25530049
MolPure® Cell/Tissue Total RNA Kit	Yeasen	19211ES60
Hifair III 1st Strand cDNA Synthesis Kit	Yeasen	11141ES10
2×SYBR GREEN qPCR MASTER MIX	Bimake	B21702
Dual Luciferase Assay Kit	Promega	E1910
ExFect Transfection Reagent	Vazyme	T101-02
Experimental models: Cell lines		
PGK12.1 (Mus., ESCs)	Provided by Dr. Tom Kerppola (Univ. of Michigan)	N/A

(*Continued on next page*)

Continued

REAGENT or RESOURCE	SOURCE	IDENTIFIER
HEK293T (Homo.)	National Collection of Authenticated Cell Cultures	GNHu17
HeLa (Homo.)	National Collection of Authenticated Cell Cultures	TCHu187
Oligonucleotides (refer to Table S1)		
Primers	Sangon Biotech	N/A
Recombinant DNA (refer to Table S1)		
pBiFC (VN- or YC-)	Provided by Dr. Tom Kerppola (Univ. of Michigan)	N/A
pMD2.G	Addgene	#12259
psPAX2	Addgene	#12260
pLKO	Provided by Dr. Jing Nan (Lanzhou Univ.)	N/A
pcDNA3.1(+)	Addgene	#78110
pGEX-6p-1	Addgene	#19322
Software and algorithms		
ImageJ	NIH	https://imagej.nih.gov/ij/

RESOURCE AVAILABILITY

Lead contact

Further information and requests for resources and reagents should be directed to and will be fulfilled by the lead contact, Bo Cheng (bocheng@lzu.edu.cn).

Materials availability

This study did not generate new unique reagents.

Data and code availability

- Original western blot images have been deposited at supplementary information and are publicly available as of the date of publication. Microscopy data reported in this paper will be shared by the lead contact upon request.
- This manuscript does not report original code.
- Any additional information required to reanalyze the data reported in this paper is available from the lead contact upon request

EXPERIMENTAL MODEL AND STUDY PARTICIPANT DETAILS

Cell culture

The mESC cell line (PGK12.1) were grown in the Dulbecco's modified Eagle's medium (DMEM, 12100046, ThermoFisher) supplemented with 15% fetal bovine serum (A9TE009, GEMINI), 0.1 mM nonessential amino acids (1628158, Gibco), 100 units/mL penicillin-streptomycin (A600135 and A100382, Sangon Biotech), 0.55 mM β-mercaptoethanol (20130110, Sigma), 2 mM L-glutamine (A100374, Sangon Biotech), and 0.1 mg/mL leukemia inhibitor factor (lab made). The cells were seeded in gelatinized (A609764, Sangon Biotech) culture dishes (Beaver). HeLa and HEK293T cell lines were maintained in the DMEM supplemented with 10% newborn calf serum (04-102-1A, Biological Industries), and 100 units/mL penicillin-streptomycin. All cell lines were cultured at 37°C in humidity-saturated 5% CO_2 atmosphere.

METHOD DETAILS

shRNA-mediated knockdown

shRNA constructs targeting *Cbx7C* (#1: GCCTCTGAGCCTTCTGCCTCG; #2: GCCCTGCCCAACCCTGCCTTG) or negative control (*shNC*: TCACCAAGGAGACTGCTATTT) sequence were generated by introducing core sequences into pLKO plasmid. These shRNA lentiviruses were packaged by transfecting 10 cm dish HEK293T cells with 3 μg of PMD.2G glycol protein-expressing vectors, 6 μg of lentiviral packaging constructs PAX2 and 6 μg of shRNA constructs utilizing ExFect Transfection Reagent (T101-02, Vazyme) according to the manufacturer's instructions. After 48 h post transfection, the collected shRNA lentiviruses within the supernatant were filtrated with a 0.22 μm filter and centrifuged at 3000 rpm. The wild type mESCs were infected with *shNC* and *shCbx7C* lentiviruses respectively. The puromycin were added to each group after 36 h post infection to screen the cells expressing shRNA for another four days before EB formation assays.

Generation of stable cell lines

For the generation of the mESC cell lines stably harboring and inducibly expressing the CBX7-EGFP-Flag, we first amplified the *Cbx7A* or *Cbx7C* sequences from the cDNA of mouse spleen tissue and inserted it into the downstream of pCMV promoter sequence within the pcDNA3.1-TRE-pCMV-EGFP-Flag vector to generate pcDNA3.1-TRE-pCMV-CBX7A or CBX7C-EGFP-Flag. The pcDNA3.1-TRE-pCMV-EGFP-Flag vector was reformed by inserting the inducible element TRE amplified from the commercial pTripZ vector into the front of the minimal pCMV promoter. Then, the expression vector was linearized and transfected into the mESCs via electroporation (ECM830, BTX) following the instructions of the manufacturer (http://btxonline.com). 1 mg/mL G418 (A100859, Sangon Biotech) was used to screen stable transfected cells 48 h post transfection and positive clones survived was isolated and further verified upon Doxycycline-treatment at 1 μg/mL for 48 h (Doxycycline [2431450, Biogems]).

BiFC assays

The BiFC vectors were constructed via the in-frame insertion of the coding sequences of *Cbx7* or the indicated factors in VN or YC BiFC plasmids (gifts from Dr. Tom Kerppola, the University of Michigan). VN encoded the N-terminal 172 amino acids of the Venus/EGFP, and YC encoded the C-terminal amino acids 173 to 238 of the yellow fluorescent protein. HEK293T or HeLa cells seeded into 6-well plates were co-transfected with the pBiFC plasmid pairs as indicated, 2 μg each, and imaged with a fluorescence microscope at 36 h post transfection (488 nm excitation, 10×).

Pull-down assays

The full-length coding sequences of CBX7A, CBX7C, RING1B, and PHC2 were inserted downstream of either the GST tag of pGEX-6p-1 vector or His tag of pET-28a vector for the expression of GST-CBX7A/CBX7C or His-RING1B/PHC2 and their truncation mutants. The fused constructs were transformed into *Escherichia coli* Rosetta strain for protein expression.

For GST pull-down assays, the GST-tagged recombinant proteins were purified with the BeaverBeads GSH (70601, Beaver) according to the manufacturer's instructions. The magnetic GSH beads bound with GST alone or GST-proteins (CBX7A or CBX7C) were washed with the washing buffer (140 mM NaCl, 2.7 mM KCl, 10 mM Na_2HPO_4, 1.8 mM KH_2PO_4, 2 mM dithiothreitol, 1.5% Triton X-100, and 1 mM PMSF, pH 7.4) for five times. Then, the equivalently His-proteins (RING1B or PHC2) were incubated with pre-washed GST-bound or GST-protein-bound GSH magnetic beads in the lysis buffer (140 mM NaCl, 2.7 mM KCl, 10 mM Na_2HPO_4, 1.8 mM KH_2PO_4, and 1 mM PMSF, pH 7.4) for 2 h at 4°C with gentle shaking. After incubation, the magnetic beads were washed twenty times with the washing buffer. The magnetic beads were boiled with 2×SDS loading buffer for 10 min, and then proteins pulled-down by GSH magnetic beads were subjected to western blot analysis with anti-His (lab-made antibody) and anti-GST (M20007, Abmart) antibodies.

The similar strategy was used to analyze the interaction between different truncations of CBX7 and full length of PHC2 using His pull-down assays. The His-PHC2 protein expressed in *Escherichia coli* were dissolved in binding buffer (20 mM phosphate buffer, pH 7.4, 500 mM NaCl, 20 mM Imidazole, and 1 mM PMSF) and bound with the BeaverBeads IDA-Co (70502, Beaver) according to the manufacturer's instructions. After being washed with the washing buffer (20 mM phosphate buffer, pH7.4, 500 mM NaCl, 20 mM Imidazole, and 1 mM PMSF) for five times, the magnetic beads bound with His-PHC2 protein were equally divided and further incubated with different truncations of GST tag-CBX7 for 2 h at 4°C with gentle shaking. Then, the magnetic beads were washed for ten times with the washing buffer. To achieve better removal of the non-specific binding proteins on the magnetic beads, we added tiny amounts of the reduced glutathione (0.05 mM) in the washing buffer. The harvested magnetic beads were mixed with 2×SDS loading buffer and boiled for 10 min, then western blot analyses were performed with His and GST antibodies.

Production of CBX7C polyclonal antibody

A partial cDNA fragment that encodes from V83 to the stop codon of Cbx7c was sub cloned into the pET28a vector to express a His-SUMO-CBX7C (83–166 aa) fusion protein. This fusion protein was purified with the BeaverBeads IDA-Co (70502, Beaver) according to the manufacturer's instructions, and then injected three times into rabbits to generate collect antiserum at the Biodragon company. For Antibody affinity purification next, the collected CBX7C antiserum were purified with the GE-CNBr activated Sepharose 4B (71-7086-00, GE Healthcare) according to the manufacturer's instructions. The efficiency and specificity of the antibody was tested in WB assays and we confirmed that it did not recognize SUMO tag, or CBX7A or CBX7B.

Co-immunoprecipitation assays

The mESCs induced expressing CBX7C fusion proteins were collected without or with 1 μg/mL Dox-treatment more than 48 h. About 5×10^7 of mESCs were lysed in a high salt buffer (300 mM NaCl, 20 mM Tris-HCl, 0.5 mM EDTA, 1 mM Na_3VO_4, 50 mM NaF, 1% NP-40, 1% Triton X-100, 1 mM PMSF, and EDTA-free mini-Tab, pH 8.0) for 2 h at 4°C. After a centrifugation for 20 min at the maximum speed at low temperature to remove cell debris, 5% of the soluble material was taken and saved as input and the rest were incubated overnight with corresponding antibodies (IgG [BF01001, Biodragon], FLAG tag Antibody [M20008, Abmart], RING1B Antibody [5694, CST]). Meanwhile, ads Protein A/G (22202, Beaver) were washed with PBS for three times according to the manufacturer's instructions, and then incubated in PBS containing 4 mg/mL BSA (A602449, Sangon Biotech) at 4°C with gentle shaking overnight to reduce the binding of non-specific proteins. After that, the antibody containing cell lysate were incubated with blocked beads for 4 h at 4°C with gentle shaking. Immunoprecipitated materials

were washed for three times with high salt buffer, and finally resuspended with 80 μL 2×SDS loading buffer and boiled for 10 min before western blot analysis.

Chromatin immunoprecipitation and qPCR assays

Chromatin immunoprecipitation (ChIP) assays were performed as previously reported.[65] The mESCs induced expressing CBX7C fusion proteins were collected without or with 1 μg/mL Dox-treatment more than 48 h. About 5×10^7–1×10^8 of mESCs were used for each immunoprecipitation. Antibodies used were listed as follows. Flag (M20008, Abmart), CBX7A (ab21873, Abcam, both CBX7A and B can be recognized), RING1B (5694, CST), PCGF2 (ab17327, Abclonal), H3K27me3 (PTM-622, PTM BIO), H2AK119ub (8240, CST). Commercial protein A/G magnetic beads (22202, Beaver) were employed. The obtained ChIP materials were treated with RNaseA (RL4250, TransGen Biotech) and Protease K (25530049, ThermoFisher) respectively for q-PCR analysis.

Fluorescence recovery after photo bleaching (FRAP)

For FRAP assays, HeLa cells expressing VN-CBX7C and YC-PHC2 simultaneously or CBX7-EGFP-Flag individually were seeded onto coverslips inside of a culture dish. Images of cells were acquired using laser scanning confocal microscopy (LSCM [A1R + Ti2-E, Nikon]) in 100-fold magnification and further zoomed in for 5-folds. FRAP imaging was performed with excitation wavelength at 488 nm, and one image were taken before photobleaching. Immediately after photobleaching with 2% of 488 nm laser in the selected square area, images were taken with 1-min intervals (expressing VN-Cbx7C and YC-Phc2) or with 10-s intervals (expressing CBX7-EGFP-Flag). Meanwhile, NIS-Elements software was used to collect the fluorescence values of the bleached area in real time. The fluorescence intensities before photobleaching were normalized before calculating the fluorescence recovery.

Embryoid bodies preparation assays

We prepared Embryoid bodies (EBs) with mESCs using the hanging-drop method (with 1500 cells/drop). Firstly, Normal cultured mESCs were digested from dishes and obtained single cell suspension and washed cells twice with PBS. Collected cells were resuspended to about 6×10^4–1×10^5 cells/mL concentration (with 1500 cells/drop) with differentiation medium without LIF after being. The above cell suspension was put into drop by drop with 25 μL on the dish cover before turned over and cover it on the 10 cm dish containing 10 mL PBS, and put it into the incubator. After 24 h, the white granular embryoid bodies formed in the liquid drop were sucked out using the micro pipette carefully and transferred to the dish containing the differentiation culture medium without LIF for further culture. EBs at different time points obtained were conducted the subsequent qPCR and west blot detection, or image by microscope. The average diameters of the EBs were calculated using ImageJ software.

Quantitative real-time PCR

Total RNAs were isolated from various organs of C57BL/6 adult mouse using an MolPure Cell/Tissue Total RNA Kit (19211ES60, Yeasen). RNA concentration was quantified by Nanodrop (Thermo Scientific, US). cDNA was processed with DNase treatment and reverse transcription from 1 μg total RNA using the Hifair III 1st Strand cDNA Synthesis Kit (11141ES10, Yeasen). Reverse transcription was performed on a metal bath at 25°C for 5 min, 55°C for 15 min and then 85°C for 5 min. RT–PCR was processed for 45 cycles on an ABI-Q5 (Life technologies) with denaturation at 94°C for 15 s, annealing at 60°C for 15 s, and extension at 72°C for 30 s using 2×SYBR GREEN qPCR MASTER MIX (B21702, BIMAKE). Primer sequences used for this experiment are shown in Table S1. Quantitative assessment of RNA levels was performed using the ABI-Q5. Relative mRNA expression was normalized to *Gapdh* (See Table S1).

Immunofluorescence assays

For immunofluorescence (IF) assays, cells were grown on coverslips placed in a 24 well culture dish. They were fixed with 4% formaldehyde for 20 min at room temperature and washed three times with PBS. And then after permeabilized with 0.5% Triton X-100 for 20 min at room temperature. The coverslips with cells were washed three times with PBS again and incubated with 5% BSA for 1 h at room temperature. Cells were then incubated with corresponding antibody (1:200 diluted in TBST) at 4°C overnight. After being washed for three times with TBST, the cells were subjected for secondary antibody (Goat-*anti*-Rabbit IgG/Alexa Fluor 594 [ab150116, Abcam]) incubation for 1 h at room temperature. The cells were further stained with 1 μg/mL of Hoechst 33342 (C0031, Solarbio Life Sciences) for 10 min and confocal images were taken in 100-fold magnification and zoom in for 5-folds.

Reporter assays

For classical Dual-luciferase reporter assay, 2 μg plasmids of GAL4 DNA binding domain (GAL4-DBD) alone, or fused with either CBX7 isoforms or PHC2 were transfected into an HEK293T cell line stably expressing Firefly Luciferase. Renilla luciferase was co-expressed with the GAL4-DBD proteins and facilitate the normalization of the transfection efficiency among samples. Cells were harvested at 36 h post transfection and the levels of both Firefly luciferase and Renilla luciferase were assayed with the Dual Luciferase Assay Kit (E1910, Promega) and measured using a GloMax 20/20 Luminometer (E5311, Promega).

For the reporter assays shown in the supplemental information, a *GAL4* binding element array was fused to the *hCYP26A1* promoter located upstream of the *EGFP-Flag* reporter gene. Meanwhile, the plasmids expressing either GAL4-DBD alone or fused with CBX7A or

CBX7C were constructed. 2 μg of the plasmid expressing the EGFP reporter and the indicated GAL4-DBD effectors were sequentially transfected into HEK293T cells with 36 h apart using Exfect Transfection Reagent (T101-02, Vazyme) following the instructions of the manufacturer. Cells were harvested 48 h after the second transfection and the expression of the reporter was assayed with western blot. TUBULIN was used as an internal reference protein.

QUANTIFICATION AND STATISTICAL ANALYSES

Statistical analyses have been clearly described in the main text, figure legends and methods, including the statistical tests, sample numbers, standard errors of the mean (SEM) and P-values, etc. Student's t test and ANOVA followed by Duncan's multiple range test ($p < 0.05$) were conducted with SPSS. Data from the biological repeats were presented as mean SEM. $p < 0.05$ was considered to be statistically significant and represented as asterisk (*). $p < 0.01$ and $p < 0.001$ were considered to be more statistically significant and represented as double asterisks (**) or triple asterisks (***), respectively. $p < 0.0001$ was considered to be the most statistically significant and represented as four asterisks (****).